Reanalysis-based mesoscale wind maps for the design of structures and infrastructures with an application to Italy

(Article begins on next page)

Reanalysis-based mesoscale wind maps for the design of structures and infrastructures with an application to Italy

Lorenzo Raffaele *, Luca Bruno, Elisabetta Colucci

GeoWindy R&D group, Department of Architecture and Design, Politecnico di Torino, Viale Mattioli 39, Torino, 10126, Italy

ABSTRACT

Synoptic extreme winds are traditionally mapped at the lower bound of the countrywide macroscale resolution (hundreds of km) on the basis of time series measured at land anemometric stations, while the assessment of the design wind speed at the construction site is entrusted to the designer within the so-called return criterion. Coarse, uneven distribution of the stations, uncertainties in their setup, measurement errors, challenging subjective evaluation of the exposure roughness, inconsistencies among national wind provisions are some of the critical issues affecting the in force map-and-return approach. This study is intended to test an alternative approach to directly assess the wind hazard at the lower bound of the meso-γ scale resolution (about 2 km) around a construction site. The approach is grounded on data issued from a weather forecast computational model, its reanalysis by means of assimilated remote sensing observations, and possibly its downscaling. Three different reanalysis/downscaling models are adopted. The resulting wind maps over the Italian Country are critically compared with measurements at 21 stations. The errors made by each model are assessed for current and extreme wind speed with different return periods. Finally, a reanalysis-based engineering approach to design wind speed is presented by proposing model correction factors.

1. Introduction

The determination of the design wind speeds is the first and key constituent ring of the 'Alan G. Davenport Wind Loading Chain' (Davenport, 1961) that still grounds contemporary Wind Engineering (Isyumov, 2012; Picozzi et al., 2024). The design wind speed at a given site is traditionally and still obtained by means of a two-stage, forth-and-back approach. The first stage is transparent to the designer, and consists in zoning the synoptic extreme winds at the lower bound of countrywide macroscale resolution (hundreds of km) on the basis of suitable extreme statistics of time series of records measured at land anemometric stations. The stage includes the acquisition, correction, transformation and probabilistic analysis of the measurements (see e.g. Ballio et al., 1999; Safaei Pirooz et al., 2021, for applications to Italy and more recently to New Zeland, respectively). Resulting wind maps are made available to designers in standards (see e.g. DM 17-01-2018, CNR-DT 207 R1/2018, AS/NZS 1170.2:2021, for the Italian and New Zeland in force standards, respectively). The second step is conversely directly entrusted to the designer by means of the so-called 'return criterion' (Ballio et al., 1999), in order to recover from the reference mapped speed (also called v_{b0} in e.g. EN 1991-1-4:2005) the design value (also referenced to v_m in e.g. EN 1991-1-4:2005) accounting for the site and construction local characteristics, i.e. altitude above the

sea level, aerodynamic roughness, orography and distance from the shoreline, reference height of the construction. The basic principles of the approach above were laid out in the early Sixties by Davenport (1960), further developed during the 20th century and applied in different Countries by other funding fathers of Wind Engineering (e.g. Solari, Ballio et al., 1991a,b, 1999, in Italy). It should be considered as the accomplishment of a pioneering and brilliant modelling effort to provide a practical design tool based on relatively scarce, uneven, point-wise anemometric measurements available at that time. In spite of such an effort, both stages of the 'map-and-return' approach are affected by some weaknesses early pointed out by Davenport himself (Davenport, 1960), and later faced by scholars in a panoply of informing studies. Selected critical issues judged as relevant to this study are reviewed in the following not necessarily exhaustive list.

Map stage: Anemometric measurements. Coarse, uneven distribution of the stations, uncertainties in their setup and measurements errors are among the main critical issues in measurement harvesting.

The averaged horizontal resolution in terms of mean distance among the closest anemometric stations $\overline{L}$ over the portion of Earth surface of interest, e.g. a single Country, is often coarse. As an example, Fig. 1(a)

---

* Corresponding author.
E-mail address: lorenzo.raffaele@polito.it (L. Raffaele).

Nomenclature

a	Angular coefficient of linear regression
cov	Coefficient of variation
h	Height above the ground
lat, lon	Horizontal geographic coordinates
r	Horizontal radial coordinate
t	Time
x, y	Horizontal cartographic coordinates
z	Elevation above the sea level
z_0	Aerodynamic roughness
A	Tributary area of an anemometric point
C	Compliance index
I_v	Time series completeness inconsistency index
I_s	Steadiness of station setup inconsistency index
I_t	Uniformity of orography inconsistency index
I_r	Uniformity of roughness inconsistency index
I_h	Anemometer height inconsistency index
L	Horizontal resolution in cartographic coordinates
T	Duration of the time series
T_R	Return period of the wind speed
$\overline{V}$	Averaged wind speed
V_m	Missing wind speed data
V_{my}	Missing wind speed data per year
V_i	Invalid wind speed data after quality control
V_c	Wind calms
V_{cy}	Wind calms per year
V_{T_R}	Wind speed associated to the return period
V_t	Anemometer wind speed starting threshold
$\overline{V}_d$	Daily averaged wind speed
$\overline{V}_y$	Yearly averaged wind speed
$\widehat{V}_y$	Yearly maximum wind speed
Δh	Difference between the actual and the reference height of an anemometer
Δt	Time step in REA models
Δt_a	Averaging period
Δt_s	Sampling period
ΔV	Anemometer resolution
γ_m	Model correction factor
$\varepsilon_{\alpha-\beta}$	Relative error of the generic dataset α with respect to β
θ	Spatial resolution in geographic coordinates
μ	Weighting factor
$\cdot_{ref}$	Reference value of the generic parameter
$\overline{\cdot}$	Mean value of the generic variable
$\widetilde{\cdot}$	Standard deviation of the generic variable
$\widehat{\cdot}$	Maximum value of the generic variable
#	Cardinality of an ensemble

Fig. 1. Country-averaged spatial resolution $\overline{L}$ of the anemometric stations used to define national design wind speed maps. Sorting in decreasing order of the Country land area: Canada (Hong and Ye, 2014), China (Mo et al., 2015), Australia (Spassiani and Mason, 2021), France (Sacré, 1993), Germany (Kasperski, 2002), Italy (Ballio et al., 1991a,b, 1996, 1999), New Zeland (Safaei Pirooz et al., 2021), United Kingdom (Cook and Prior, 1987), Ireland (Logue, 1989) (a); Voronoi cells around the anemometric stations adopted to map the extreme winds in Italy (processed after Ballio et al., 1996, 1999, 42 stations of the Italian Military Air Force ITAV, 27 stations of the Italian Electric Power Company ENEL) (b); statistics (boxplot) of horizontal resolution of the stations L (c).

reviews $\overline{L}$ adopted to define national extreme wind speed maps in 9 Countries.

The worldwide mean value $\overline{\overline{L}}$ has the order of magnitude of 100 km, while the Europe-averaged one is around 66 km. L is often also not uniform over a single Country. As an example, Fig. 1(b) maps the Voronoi tessellation of the Italian land with reference to the 69 stations used to define the Italian extreme winds (Ballio et al., 1996, 1999), and draws the boxplot of $L_i = \sqrt{A_i}$, where A_i is the area of the ith cell. Small islands apart, the resolution varies in the range [7,110] km, with a single lower outlier corresponding to the cell around the
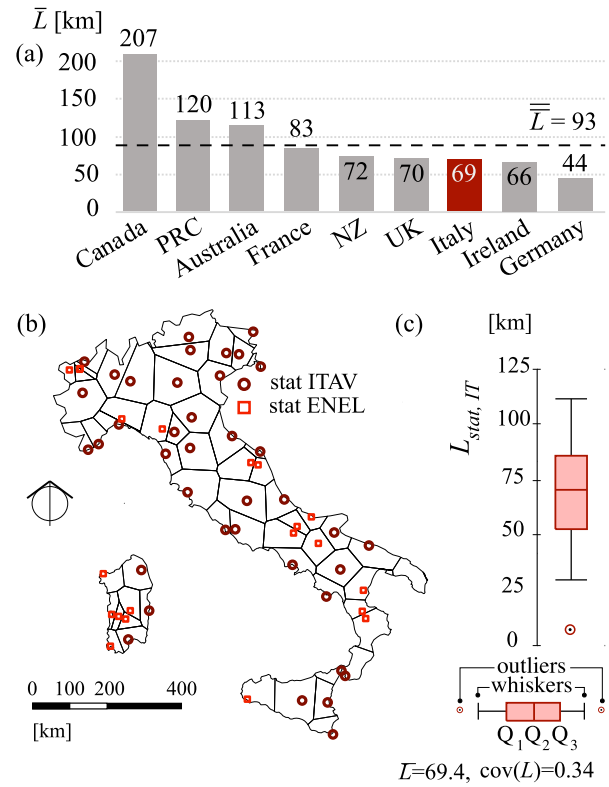
station of Trieste lanterna. The coefficient of variation is not negligible in Italy (cov(L) = 0.34), but the variability seems even higher in larger Countries with uneven population density, e.g. Canada (Hong and Ye, 2014, Fig. 1) or PRC (Mo et al., 2015, Fig. 2).

The extent of the measurement time windows T is usually shorter than the target return period T_R of the design wind speed V_{T_R} of interest (Solari and Pagnini, 2009). As an example, Fig. 2(a) reviews the time windows $\overline{T}$ averaged over the anemometric stations used to define national design wind speed maps in the 9 Countries previously referenced in Fig. 1. The worldwide mean value $\overline{\overline{T}}$ is around 30 years. As a result, T does not necessarily secure the statistical convergence of the design wind speed of interest.

The extent of the measurement time window T is often not homogeneous among stations. As an example, Fig. 2(b) graphs the time windows T available at the anemometric stations adopted to draw the Italian map of extreme winds (Ballio et al., 1996, 1999).

The sampling period Δt_s and the averaging one Δt_a are not necessarily homogeneous among stations and/or not constant along T (e.g. 10', 1-h, 3-h or 6-h, Picozzi et al., 2022). It follows that the time window needs to be further reduced to secure homogeneous data. Alternatively, data can be corrected in the attempt to make it homogeneous, even if a general criterion based on first principles is not yet available (Picozzi et al., 2022).

The datasets of the collected measurements should be regularly and systematically updated in order to include recent severe wind events, not necessarily but possibly due to climate change (Dunn et al., 2019;
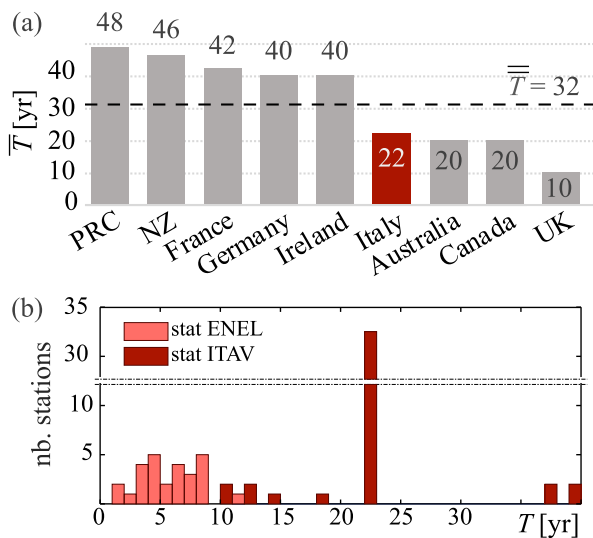
Fig. 2. Country-averaged duration $\overline{T}$ of the time series used to define national design wind speed maps (a, see Fig. 1 for data sources), T at each of the anemometric stations adopted to draw the Italian map of extreme winds (b, processed after Ballio et al., 1996, 1999).

Rapella et al., 2023). A rare historical example of single update was carried out by Sacré (2000) and Sacré (2002) in order to revise the previous extreme wind map over France (Sacré, 1993) in the wake of the wind storm occurred on Dec. 1999.

In spite of the guidelines in WMO-No. 8/2021, the actual anemometer performances affecting the measurements are not necessarily homogeneous in space and not constant in time (Liu et al., 2024), e.g. their type (e.g. pressure-plate, cup, or 2D sonic anemometers, Mo et al., 2015; Picozzi et al., 2022), their model (Azorin-Molina et al., 2023) and related specifications, e.g. their speed starting threshold value $V_t \approx$ 1 m/s artificially affecting wind calms ($V_c < 0.2$ m/s, WMO-No. 8/2021, Chiodi and Ricciardelli, 2014; Liu et al., 2024), their measurement resolution $\Delta V \approx 0.5$ m/s, their deterioration during the service life, e.g. dust-induced friction increase (WMO-No. 8/2021, sect. 5.10), their data acquisition chain whose malfunctioning is responsible for missing data V_m (Picozzi et al., 2022).

Although anemometers should stand at 10 m height above the ground and located in level open terrain (WMO-No. 8/2021), their actual location and eventual relocation (Liu et al., 2024), height above the ground h and the aerodynamic roughness z_0 of their neighbourhoods are not necessarily standard and constant in time. To the Authors' best knowledge h is not systematically provided in international anemometric databases (e.g. in the global dataset NCEI, 2023), and in scientific papers devoted to extreme wind speed mapping (with notable exceptions, e.g. Ballio et al., 1999). Analogously, the assessment of the effective aerodynamic roughness needed for correction/homogenization is not a trivial task, often subjective and visual-survey-based in morphological methods (Grimmond and Oke, 1999; Shen et al., 2022), and in particular for stations with very non-homogeneous azimuth-wise fetch conditions in a range of 2 km around the station. Finally, z_0 can strongly vary in time due to seasonal changes of the tree leaf density (Dolman, 1986), and/or to rapid urbanization growth (Mo et al., 2015).

Map stage: Control, transformation and statistical analysis. The Quality Control (QC) of increasingly huge amounts of anemometric measurements is both a mandatory, not trivial and demanding task (Lott, 2004; Dunn et al., 2012). As a recent example, Rojas-Labanda et al. (2023) discussed in deep the QC methods for surface wind data from heterogeneous origins, applied them over Europe setting the first version of the EuSWiO database, and obtained stunning results in terms of e.g. intra-

and inter-site duplication of a number of stations (see Rojas-Labanda et al., 2023, Fig. 2–3), related invalid measurements and remaining valid ones.

Multiple statistical models are used for conventional Extreme Value Analysis (EVA) of controlled wind speed data, under the common assumption of stationarity (see e.g. Gomes and Guillou, 2015, for a full review). Among them, the most widespread in Wind Engineering include the Extreme Value Theory and related Gumbel, Fréchet, Weibull or Generalized Extreme Value asymptotic distributions, and the Peaks Over Threshold (POT) method and related Generalised Pareto Distribution (GPD). Their assumptions, historical development and controversial performances in wind engineering are critically reviewed in deep by e.g. Torrielli et al. (2013) and Chiodi and Ricciardelli (2014).

Map stage: Wind zoning. Each Country has developed and applied different procedures for anemometric data measuring, control, transformation and probabilistic analysis. Moreover, different types of territorial maps have been utilized in national standards, namely continuous isocontour maps of the wind speed or discontinuous ones referring to geographical limits (e.g. rivers) or administrative borders (Ballio et al., 1991a). The sum of the above "*have invariably led to a set of national design wind speed maps with significant* [and physically unjustifiable - ed.] *discontinuities in wind speeds at national* [and inner administrative -ed.] *borders*" (Miller, 2003). Such an issue remains unsolved 20 years later at the dawn of the Second Generation Eurocode on wind actions on structures, as recently pointed out by Ricciardelli (2023).

Return stage. The designer entrusted of this stage must face multiple issues affecting the evaluation of the design wind speed induced by the site features. Among them, the challenging subjective evaluation of the aerodynamic roughness z_0, the variations among different terrain categories and related z_0 values in codes and standards, and the difficult estimate of the effects of local terrain orography. On the first point, Lettau (1969) early stressed the problem to estimate a z_0 value strictly based on a visual site survey, even using measurement metrics to describe the characteristic roughness elements. Much more recently, Yu et al. (2023) have extensively reviewed the exposure roughness specified in current wind codes and standards, pointed out ambiguity and discrepancies, and recognized the wind exposure as one of the most intricate issues for wind engineering, resulting in the significant uncertainty of wind load evaluation. It is difficult for the designer to unambiguously connect the construction site to terrain categories often qualitatively described in codes and standards (e.g. EN 1991-1-4:2005, CNR-DT 207 R1/2018, Annexes A1 and C, respectively), adopt a z_0 value face to different provisions for the same nominal terrain category (e.g. $z_0 = 0.003$ m and $z_0 = 0.01$ m for coastal areas in EN 1991-1-4:2005, DM 17-01-2018, respectively), and refer to simplified 2D scenarios (e.g. the ones provided in EN 1991-1-4:2005, Annex A.3) to evaluate the local effects of real-world, 3D orography.

It is useful to note that each of the critical issues reviewed above can be viewed as a source of measuring or modelling errors that affects the evaluation of the design wind speed.

In order to cope with most of the difficulties related to the map stage grounded on land anemometric stations, Miller (2003) was the first to take up a concept already suggested by Davenport (1965): reference is initially made to mean sea level pressure maps, then geostrophic wind speed is derived, its extreme value statistically analysed, and finally converted to equivalent 10-min average wind speeds at 10 m above the surface by using the geostrophic drag law through the assessment of the friction velocity. The Miller's approach has the unquestionable advantage to exclude the uncertainties affecting the setup of the anemometric stations and to overcome the inconsistencies among national wind maps. Nevertheless, the results heavily depend on the adopted value of the uncertain dimensionless model parameters in the geostrophic drag law. In other words, epistemic uncertainties which had been let out of the door of the anemometric stations are brought back through the window of the geostrophic drag law. More interestingly, in the same

paper, Miller (2003) outlines possibilities for future works, and cites as an alternative approach the use of the nascent reanalysis of numerical weather predictions, such as the first ERA-15 dataset issued by the European Centre for Medium-Range Weather Forecasts (ECMWF). In spite of his visionary preview, Miller's foresight has received very little attention in Wind Engineering to date, with few remarkable exceptions to our best knowledge.

Mo et al. (2015) followed the same approach in Miller (2003), but mean sea level pressure maps are obtained by NCEP/NCAR Reanalysis 2 dataset (horizontal resolution $\theta = 2.5°$, $L \approx 278$ km, time resolution $\Delta t = 6$ h). More recently, two studies have almost simultaneously exploited the reanalysis approach and modern datasets to directly obtain the wind velocity. Yang et al. (2022) adopted the ECMWF/ERA5 dataset to recover the current wind speed and direction as a basis for the analysis of the vortex shedding-induced fatigue of overhead transmission line conductors. The implications of such a specific goal are twofold: the very short duration of two time series ($T = 1$ month each) because extreme winds are not of interest; the further downscaling of the ERA5 data (native horizontal resolution $\theta = 0.28°$, $L \approx 31$ km) to assess the wind conditions along the line-like infrastructure far from land stations and in between successive ERA5 grid points. A deterministic interpolation (namely, the Inverse Distance Weighting method) and a mass-conserving simplified dynamical model (namely, WindNinja) are adopted among the available downscaling procedures. Both adopted methods allow a downscaling at an horizontal resolution $L = 100$ m over a domain equal to 50×50 km. Comparison is carried out with measurements at 9 meteorological stations from Environment Canada. Li et al. (2021) evaluated the extreme wind speed over the Arabian Peninsula by referring to two reanalysis datasets ($\theta = 1°$, $L \approx 111$ km, $\Delta t = 6$ h) further dynamically downscaled by using the Weather Research and Forecast model at a horizontal resolution $L = 4$ km over a period $T = 30$ years. Ten anemometric stations located in major cities within the region were selected for comparison. 3-second gust design wind speeds maps are finally obtained for multiple (from 50- to 3000-year) return periods.

In the wake of the above, the present study aims at shedding light on three main issues: i. Is reanalysis, eventually coupled with downscaling by deterministic interpolation, or by higher resolution climate model suitable to accurately map current and extreme winds? ii. Are reanalysis datasets suitable at all wind spatial and time scales, and at all orographical and exposure types? If not, which is their smallest threshold scale of application? iii. Can reanalysis offer the opportunity to conceive an approach to design wind mapping alternative to the in force codified two-stage 'map-and-return' approach based on land anemometric stations? If yes, what are the advantages and limitations?

In order to answer the above questions, we consider three reanalysis datasets. Their performances in predicting current and extreme wind speeds with different return periods are assessed with respect to the measurements at multiple land anemometric stations critically analysed and selected. The Italian land is adopted as a well-adapted, particularly challenging benchmark because of its geomorphological features, where roughness and orographical high variability ubiquitously occurs along extensive coastal and mountainous zones. An alternative reanalysis-based approach is finally proposed, qualitatively and quantitatively compared with the traditional codified one currently in force in Italy (DM 17-01-2018, CNR-DT 207 R1/2018).

The paper is organized into five further sections. Section 2 introduces the adopted reanalysis models and summarizes their main features relevant to the specific application. The measurements at selected land anemometric stations are carefully and critically analysed in Section 3, in order to secure a proper comparison with reanalysis. In particular, a synthetic index is proposed to quantitatively measure the compliance of each station against measurements time series duration, completeness, and standard exposure. The performances of the reanalysis models are assessed in Section 4 with respect to measurements, and the full national maps of the current and extreme winds over Italy

are provided. The reanalysis-based approach is proposed in Section 5 and its performances are compared with the ones of the in force codified approach. The specific conclusions of the study and the general perspectives of the approach are outlined in Section 6.

2. Wind modelling and reanalysis approach

The reanalysis approach, generally referred as 'REA' in the following, blends observations with past short-range weather forecasts rerun with cutting-edge weather forecasting models. It has been very recently tested and widely used to an increasing extent in multiple fields of applications, for instance renewable energy (e.g. Doddy Clarke et al., 2021), agriculture (e.g. Almendra-Martín et al., 2021), water resources (e.g. Do et al., 2020), and insurance sector (e.g. Gesualdo et al., 2024). Modern climate reanalysis has at least four main recognized potentials: i. it "*delivers a complete and consistent picture of the past weather*" (Thépaut et al., 2018), "*relying on a numerical weather prediction model to assimilate historical observations (e.g., from satellite, in situ, multiple variables) that are not homogeneously distributed around the globe*" (Raffa et al., 2021); ii. over time, it secures long term time series, eventually continuously updated to account for climate or exposure changes; iii. over space, it offers '*maps without gaps*' having horizontal resolution higher than the codified extreme wind maps in Wind Engineering, with global worldwide covering to avoid conflicts of the national wind maps at boundaries (Miller, 2003); iv. datasets are easily accessible in open access via institutional web-based repositories to guarantee analysis repeatability. Apart from the potentialities above, the accuracy of reanalysis models versus anemometric field measurements is not univocal and currently debated, namely with respect to current wind speed in the fields of climatology (e.g. Molina et al., 2021; Doddy Clarke et al., 2021; Gumuscu et al., 2023) and renewable energy (e.g. Gualtieri, 2021, 2022). Reanalysis predictions are found to significantly depend on the quantity of interest (e.g. 1, 6, or 24-hourly current wind speed), height above the ground (the conventional 10 m level, or e.g. the height of tall wind turbine towers), exposure type (e.g. offshore, flat onshore, coastal or mountainous sites), beyond the adopted reanalysis model. In order to provide a general key to understanding such variable performances, in Fig. 3 we explicitly refer the average horizontal and time resolutions of the ECMWF REA models to the space and time scales of the atmospheric processes initially set in meteorology (Orlanski, 1975; Fujita, 1986) and well-known in Wind Engineering as well (Dyrbye and Hansen, 1996). Since the release of the first global reanalysis in 1997 (ERA-15, Gibson et al., 1997) to the very last one in 2023 (ERA5, Hersbach et al., 2020), the ECMWF models progressively refined their horizontal resolution from $L \sim 187$ km to $L \sim 31$ km, i.e. crossing the whole range of meso-β scales. Correspondingly, the time resolution increased from 6-hourly wind speed (meso-β time scale in ERA-15, -40, -Interim) to 1-hourly (meso-γ time scale in ERA5), and duration of the historical time series increased from $T = 14$ years in ERA-15 to $T = 83$ years in ERA5. In parallel, reanalysis evolved in physical models and observation assimilation systems. Thanks to such a reading key, it is clear that ERA5 reanalysis is expected to be sufficiently reliable at locations with orography and land cover homogeneous fetch over about dozens of km (lower bound of the m-β scale), such as offshore or nominally flat onshore locations (Gualtieri, 2022). However, further spatial downscaling is required to cover, both in figurative and strict use, the 'last mile', i.e. to reach the lower bound of the meso-γ scale (2 km) and potentially describe corresponding winds (e.g. thunderstorms, sea or mountain breezes) over mountainous and coastal sites, where current wind speed is under- and over-estimated, respectively, even by the best-performing global reanalysis models such as ERA5 (Gualtieri, 2022). Different approaches to regional downscaling of reanalysis are proposed in the literature, from deterministic, statistical or artificial neural network-based interpolation methods (reviewed e.g. in Hartkamp et al., 1999)
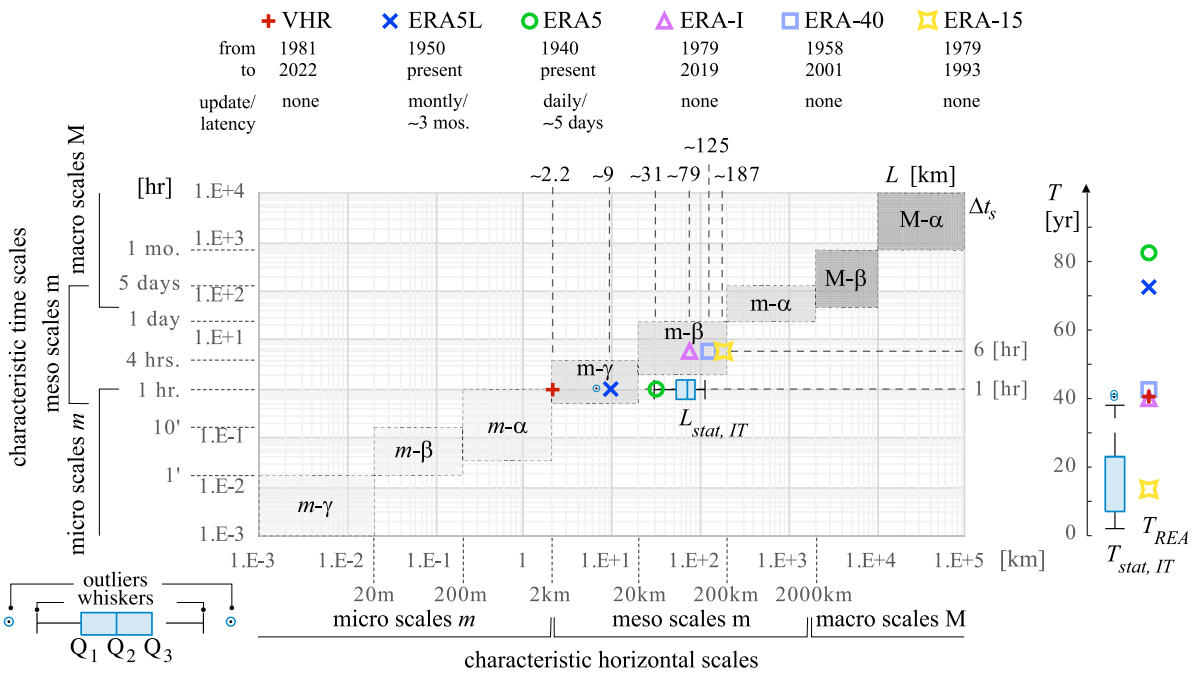
Fig. 3. Space and time scales of the atmospheric processes, synopsis of the time series duration T, horizontal resolution L and sampling period Δt_s of the reanalysis models [REA, specifically ERA-15, ERA-40, ERA-Interim (ERA-I), ERA5, ERA5-Land (ERA5L), VHR-REA_IT (VHR)], and of the Italian land anemometric stations used in Ballio et al. (1999) to draw the Italian wind map (DM 17-01-2018).

to physical-based dynamical downscaling models, e.g. diagnostic models (Ratto et al., 1994), Regional Climate Models (RCM, reviewed by Xue et al., 2014) or full convection permitting RCMs (Prein et al., 2015; Lucas-Picher et al., 2021). Among the above, two approaches move from ERA5 as input: the ERA5-Land reanalysis (ERA5L in the following) and the Very High Resolution REA over Italy (VHR-REA_IT, VHR in the following) convection permitting RCM. It is clear from Fig. 3 that both datasets are potentially able to resolve the meso-γ scale, even if to a different extent, i.e. to account for winds over sites with discontinuous roughness and orographical changes at the mesoscale. Fig. 3 also shows for the sake of comparison the statistics of the horizontal resolution $L_{stat,IT}$ and the time series duration $T_{stat,IT}$ of the anemometric stations used to set the map of the Italian extreme wind speeds. It is clear that ERA5, ERA5L and VHR models equal anemometric stations sampling period, while they are competitive to stations in terms of time series duration and of spatial resolution, i.e. able to fully cover the meso-γ scale by equal or longer observations.

The wind speed datasets considered in the present study result from the three REA models above. All the models are quite large and complex, encompassing decades of developments. The detailed description of each model is largely beyond the range and scope of this paper. In the following, reference is made to the parent papers/documentation, while only the features of the models that are considered strictly relevant to Wind Engineering are shortly described, i.e. useful to read the wind dataset issued form each model. The specific features of the three REA models are recalled first. Then, comparative analysis is carried out about common issues. For a comprehensive review of the features and relative performances of REA models besides the ones discussed here, interested readers can refer to the comprehensive survey by Gualtieri (2022), where the performances of multiple global reanalysis models (MERRA, CFSR, NCEP/NCAR R2, ERA5, among others) and several regional downscaling models (NARR, COSMO-REA2, MÉRA, HARMONIE, among others) are compared in predicting the averaged wind speed for wind energy applications.

ERA5 is the fifth generation reanalysis developed by ECMWF (Hersbach et al., 2020). It globally covers the whole Earth with a horizontal resolution equal to $\theta = 0.28°$, i.e. about $L \approx 31$ km. ERA5 combines

a numerical weather prediction model of the dynamical and moist thermodynamical state of the atmosphere with empirical observation data properly assimilated. The adopted physical weather forecast model (CY41R2) numerically solves the Eulerian velocity-based unsteady continuity, momentum, thermodynamic, and moisture equations (ECMWF, 2016a) over a horizontal Gaussian grid. The so-called parametrization schemes for radiative transfer, turbulent mixing, convection, clouds, surface exchange, subgrid-scale orographic drag and non-orographic gravity wave drag indirectly model the effects of subgrid-scale mechanisms on the large resolved scale flow (ECMWF, 2016b). Overall, about 95 billion observations were assimilated within 40 years from 1979 to 2019, i.e. 65 million per day in average (Hersbach et al., 2020). Wind observables at high altitude come from radiosondes, weather meteorological balloons, wind profilers, aircraft-based instruments. With regard to wind velocity components at 10 m height, measurements made near the sea surface on ships and drifting/moored buoys are retained only, while assimilated observations at land airport weather stations are limited to surface pressure. It follows that i. the number of worldwide daily actively assimilated observations of wind velocity components at 10 m is relatively small and equal to about 5000 in average over the period 1979–2019, and that ii. the comparison between records at land anemometric stations and reanalysis is not trivial and directly driven by assimilation. The land characteristics are described in ERA5 using several time-invariant fields, the land-sea mask, the lake cover and depth, the soil and vegetation type, and the vegetation cover among others. The above data are 4D-variational assimilated (4D-Var) within adjacent 12-hourly long time window, given a background forecast valid at the start of the window and observations falling within that window. The aim is to minimize the misfit between the observations and their modelled equivalents (Hersbach et al., 2020), also accounting for random uncertainties in both background forecasts and observations. Uncertainties are quantified from the Ensemble of Data Assimilations (EDA) system, i.e. a reduced resolution ten member ensemble (one control and nine randomly perturbed members) of short-range forecasts providing background error estimates. Observations in 4D-Var are subject to a range of quality controls, from a priori blacklisting of data known to be of poor quality, to the eventual downgrading of

observations by reducing their weight inside the minimization through variational quality control (VarQC, Hersbach et al., 2020).

ERA5L is a reiteration of the land component of the ERA5 reanalysis at a horizontal resolution equal to $\theta = 0.1°$, i.e. about $L \approx 9$ km (Muñoz Sabater et al., 2021). The physical weather forecast model adopted by ERA5L (CY45R1) is analogous to the one adopted by ERA5. ERA5L model is driven by the atmospheric forcing resulting from ERA5 near-surface meteorology state and flux fields, including air temperature, specific humidity, surface pressure, wind speed, downward shortwave and longwave radiation and liquid and solid total precipitation. These ERA5 fields are interpolated to the 9 km resolution via a linear interpolation method based on a triangular mesh (Muñoz Sabater et al., 2021). Among them, temperature, humidity and pressure fields are also corrected to account for elevation differences between ERA5 and ERA5L topographies resulting from the higher resolution. In other words, the above fields (wind speed included) shall be read as an interpolated input of ERA5L while they are not downscaled by the physical weather forecast model.

VHR results from dynamical downscaling of ERA5 reanalysis to the so-called convection-permitting scale allowing for explicit resolution of convection on the model grid (Raffa et al., 2021). Initial conditions and lateral boundary conditions (updated every 3 h) are set by interpolating ERA5 data from the ERA5 coarse grid to the finer VHR grid. Time dependent relaxation boundary conditions allow to force the solution at the lateral boundaries without causing numerical noise propagation (Doms and Baldauf, 2013). The regional downscaling covers a domain around Italy (lon = 5°: 20°E, lat = 36°: 48°N) with a horizontal resolution equal to $\theta = 0.02°$, i.e. about $L \approx 2.2$ km. Convection-permitting regional climate models are gaining broad attention from the climate community, given the promising performance in simulating precipitation features and their sensitivity to climate change (Raffa et al., 2023). Furthermore, the increased horizontal resolution allows to improve the representation of fine-scale orography and roughness transitions (e.g. in correspondence of coastal zone and urban areas). The dynamical downscaling is carried out with the regional climate model COSMO-CLM, i.e. a non-hydrostatic and limited-area model designed for dynamically downscaling simulations at different horizontal resolutions varying from the meso-β to the meso-γ scales (Adinolfi et al., 2023). The COSMO model is based on the thermo-hydrodynamical equations describing compressible flow in moist atmosphere. Parametrisation schemes are adopted to account for subgrid-scale turbulence (turbulent kinetic energy closure equation based on Mellor and Yamada, 1974; Raschendorfer, 2001), precipitation, grid-scale and subgrid-scale clouds (single-moment scheme adopting five hydrometeors, Doms and Baldauf, 2013), shallow convection (Tiedtke, 1989), radiation (two-stream version of the radiative transfer equation based on Ritter and Geleyn, 1992), soil, lakes, terrain and surface data (7-layer soil model TERRA-ML, with urban physics parametrized by TERRA-URB, Doms et al., 2013; Wouters et al., 2016), also in correspondence of urbanized surfaces allowing for a better description of the dynamics over urban canopies (Adinolfi et al., 2023). Land use, surface elevation and soil type are determined through the GLC2000 (Bartholomé and Belward, 2005), GLOBE, and FAO Digital Soil Map datasets, respectively.

For the purposes of visual comparison, Fig. 4 exemplifies the grid by ERA5, ERA5L and VHR over the Voronoi cell of a single station in Italy.

All the REA models above require the setting of z_0, and assume it as homogeneous over each cell face adjacent to ground. We stress that setting the exposure is one of if not the most crucial task in the determination of the design wind speed (Yu et al., 2023), in charge of the designer in the map-and-return approach (e.g. EN 1991-1-4:2005). Conversely, REA models directly take into account the explicit mapping of z_0 over land and sea surfaces. ERA5 and ERA5L set z_0 as a function of the vegetation type over land, while the wind-wave interaction effect is considered to estimate z_0 over sea. Conversely, VHR defines
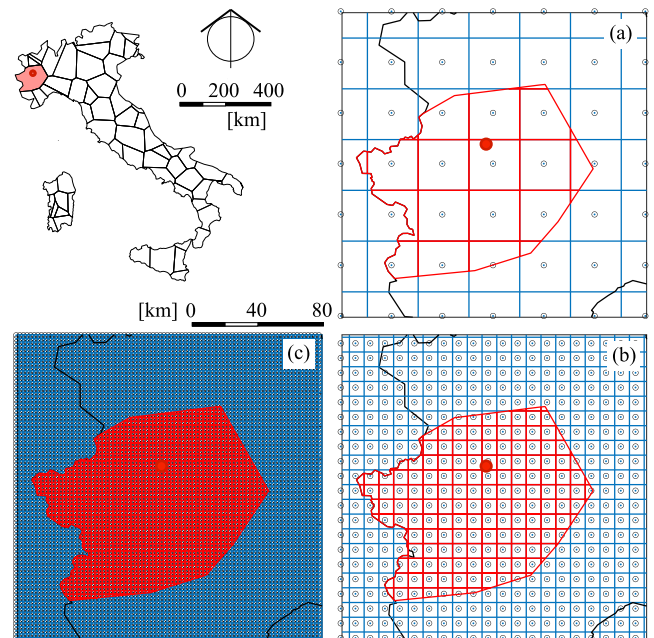

Fig. 4. Voronoi cell of the anemometric station in Torino Caselle airport, sampled by the horizontal grids of ERA5 (a, 22 cells), ERA5L (b, 169 cells) and VHR (c, 2425 cells).

z_0 as the sum of two contributions, namely, the roughness associated to subgrid-scale variance of orography according to GLOBE Digital Elevation Model (Hastings et al., 1999) and the roughness associated to the land-use category according to GLC2000 (Bartholomé and Belward, 2005). It follows that z_0 differs between ERA5 and VHR models in terms of both definition and value. To highlight such differences, z_0 is mapped according to ERA5 and VHR models in Fig. 5(a,b), respectively.

Despite the striking difference in terms of resolution, the horizontal distribution of z_0 qualitatively follows an analogous pattern, i.e. z_0 is higher in correspondence of the Alpine region and along the Apennines. Some closeup views pairing z_0 contours with the VHR cell centres of the region around Rome, and more closely around the stations of Roma Fiumicino, Genova Sestri and Trieste Lanterna are shown in Fig. 5(c,d,e,f), respectively. VHR enriches the resolution of z_0 and it is able to catch changes in z_0 induced by both vegetation and urban fabric (Doms et al., 2013). Fig. 5(c) shows how the resolution of VHR allows to clearly distinguish zones with very low z_0, such as lakes (i.e. Bracciano lake) and sea, and zones with high z_0, such as Rome conurbation and forests (i.e. Castelli Romani and Castelporziano). The closeup view of Roma Fiumicino station (Fig. 5d) shows homogeneous z_0, while the closeup views of the Genova and Trieste stations (Fig. 5e,f) reflect its rapid transition from sea, low z_0 values, to urban and forest terrain, large z_0 values.

It is worth stressing that all the REA models above are inevitably affected by assumptions and multiple potential sources of errors, as usual in Computational Wind Engineering (CWE, e.g. Bruno et al., 2023). On the one hand, physical and mathematical models inevitably take with them hypotheses and approximations. On the other hand, further approximations and related errors result from discretization methods, computational grids and numerical schemes. In the following, some REA models assumptions and potential sources of errors are mentioned.

ERA5 and ERA5L do not account for urban land surface schemes and related roughness (Lipson et al., 2022). Moreover, ERA5L and VHR consider time-constant values of z_0. It follows that the simulated wind speed is insensitive to land cover variation over time (e.g. seasonal variability of vegetation, increasing urbanization). Conversely, ERA5
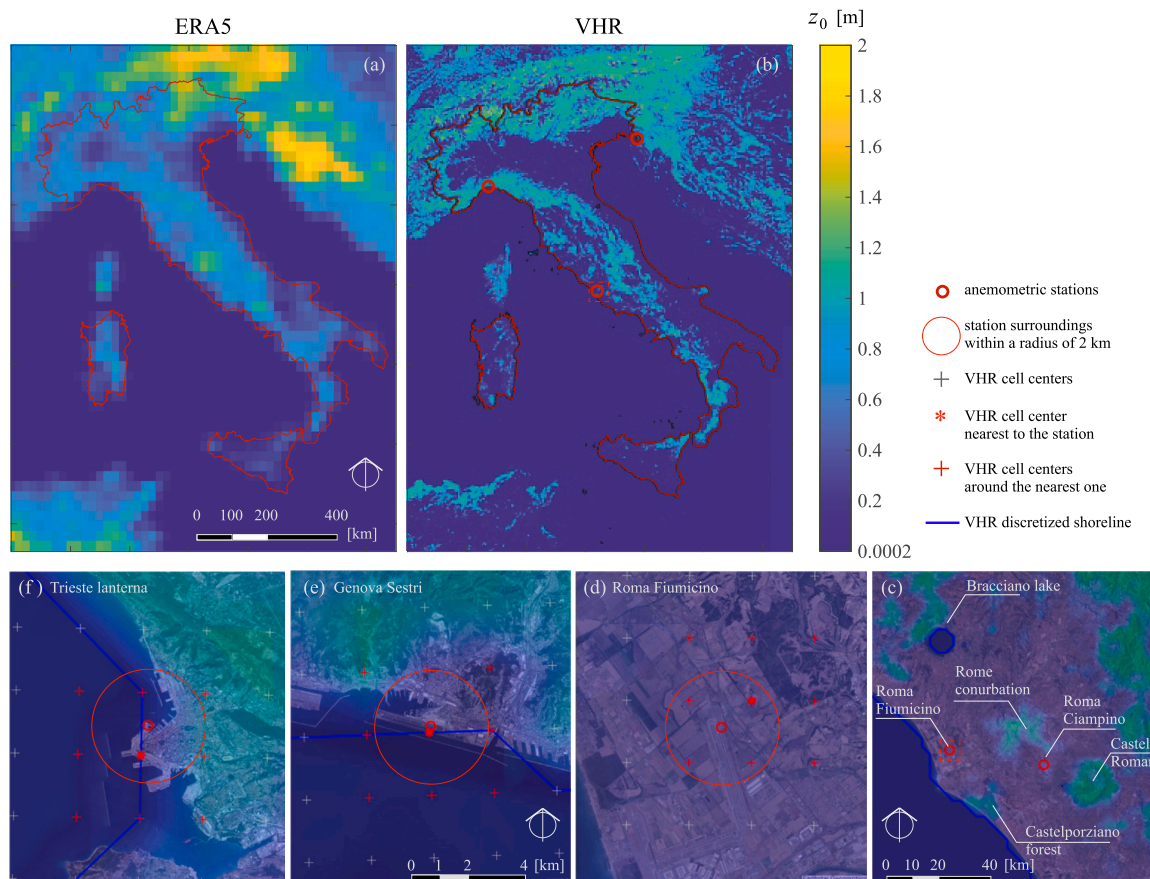
Fig. 5. Mapping of z_0 according to ERA5 (a) and VHR (b, courteously provided by CMCC Foundation). Detailed view around the whole Rome region (c), and further closeup views around the anemometric stations at Roma Fiumicino (d), Genova (e), Trieste (f).

in principle accounts for land cover variability, but slight changes are recognized for grasslands and croplands only (Peng et al., 2022).

REA mesoscale models methodically cover scales up to the meso-γ time scales only. Consistently, they do not model microscopic features in space and time that belong to microscopic scales: inhomogeneous terrain features over a single cell are neglected since z_0 is set constant over it; all REA physical models briefly described above (CY41R2, CY45R1, or COSMO) do not explicitly model grid-scale turbulence eddies, i.e. they are not scale-resolving models (Bruno et al., 2023) so that they do not natively simulate gust wind speed (e.g. 3-second gust in ASCE7, Lombardo, 2021). As such, according to WMO-No. 1555/2010 wind speeds resulting from REA computational models should be regarded as time-varying estimates averaged over the cell spatial dimension and over the time step Δt set in the numerical model. It results that the averaging period Δt_a is equal to $\Delta t_a = \Delta t = 12$ min for ERA5 and ERA5L, while $\Delta t_a = \Delta t = 20$ s for VHR. It is worth stressing that despite the much finer Δt_a within the micro-γ time scale, VHR wind speed estimates cannot account for micro meteorological turbulent fluctuations. Conversely, the sampling period Δt_s is homogeneous among the adopted REA models and equal to $\Delta t_s = 1$ h. In other terms, REA wind data are hourly-sampled wind speeds averaged within different periods, i.e. 'downsampled disjunct' according to Picozzi et al. (2022).

3. Critical analysis of the selected in situ measurements

Historical time series of in situ measurements at land anemometric stations ('stat' in the following) are adopted as term of reference to assess the relative performances of REA models in terms of I. *representativeness*, i.e. REA performances under different mesoscale types of climatic zones, site orography and exposure, and II. *relative accuracy*,

i.e. the scatter between REA results and stat measurements. 21 Italian anemometric stations are selected among the 129 available in the Met Office Hadley Centre's Integrated Surface Database (HadISD, Dunn et al., 2016; Dunn, 2019), an open access global subdaily dataset based on the ISD dataset from NOAA's NCDC (NCEI, 2023). They are mapped in Fig. 6. For the sake of brevity, the stat details are summarized in Annex - Table A.1. The a priori selection of the stations and the subsequent critical analysis of the measurements are intended to pursue both the above goals.

I. Representativeness. Station locations are primarily selected to attain the first goal on the basis of two criteria:

(I.a) they are as evenly distributed as possible over the Italian land in order to catch the largest number of climatic zones with reference to the current wind zoning defined in DM 17-01-2018, CNR-DT 207 R1/2018 (see Fig. 6);

(I.b) they are potentially representative of qualitatively different orography and exposure conditions at mesoscale: Torino, Milano Malpensa, Bologna and Firenze Peretola are located in nearly flat onshore sites; Bolzano and Monte Paganella in mountainous sites; Genova Sestri, Messina torre faro and Reggio Calabria along mountainous coastlines, the remaining stations along coastal zones with almost flat surrounds.

II. Relative accuracy. The setup and dataset of each station are further analysed to judge the comparability between them and the REA approach, as a required precondition to achieve the second goal. In a general conceptual sense, we can only be in agreement with Schatzmann et al. (1997): "*to simply compare model results with measured data is often inappropriate since data generated in field experiments and those from model simulations exhibit systematic differences [...] Such a comparison*
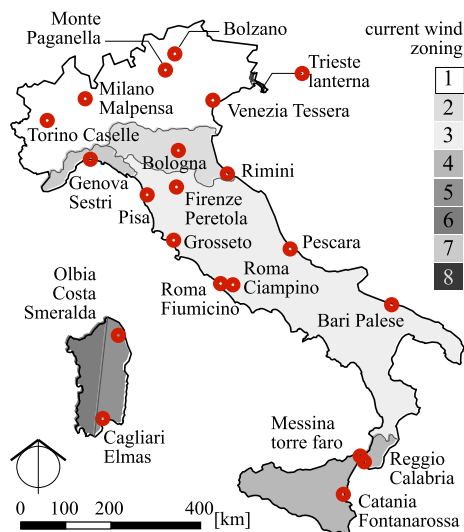
Fig. 6. Location of the 21 selected stations (detailed information in Annex, Table A.1) with reference to the current wind zoning (DM 17-01-2018, CNR-DT 207 R1/2018).

often resembles the proverbial comparison of apples with oranges." In a specific technical sense, comparability is discussed in terms of data quality and climatological representativeness at mesoscale of the stations.

(II.a) Data quality. As discussed in Section 2, the observations in ERA5 reanalysis are thoroughly quality checked. Analogously, all the stat time series from HadISD database guarantee a fully automated QC by running 15 different tests to flag the poorest records as invalid data V_i (Dunn et al., 2012). In particular, wind speed data is defined invalid in the case of months duplication, nonphysical isolated clusters of data, discrepancies into temperature diurnal cycle, exceedances of observations beyond limits based on documented records, consecutive observation replications, low reliability due to low cardinality of monthly records.

(II.b) Station WMO-compliance. REA models do not inherently change in time, do not systematically account microscales because of their maximum resolution in time and space (Fig. 3), and the resulting datasets are standardized and without gaps. Conversely, the above stat dataset QC does not necessarily secure the compliance of the station actual setup with the ideal one defined by the WMO-specifications, i.e. a constantly accurate, properly maintained, 10 m high anemometer above a level, open, unobstructed terrain with constant and uniform roughness in the 2 km radius fetch upwind the station (WMO-No. 8/2021). The stat WMO-compliance is clearly not trivially guaranteed in the light of the previous studies on the weaknesses of the map stage we reviewed in Section 1. In a scale-based reading key, WMO specifications within the 2 km radius fetch are intended to secure the "*climatological representativeness*" (Wieringa, 1996) of the measurements at the meso- and macro- scales by avoiding local microscales and their contribution to wind speed. Here we critically discuss and quantify the discrepancies, if any, between the actual setup/measurements of the selected stations and the WMO provisions. In such a way, we also indirectly point out the possible systematic differences between REA and stat datasets. In order to do so, we propose a synthetic compliance index $C \in [0, 1]$ in its very general form as

$$C = 1 - \frac{\sum_{j=1}^{n} \mu_j I_j}{n}, \tag{1}$$

where $I_j \in [0, 1]$ are n partial, maximum-normalized inconsistency indices related to time series completeness ($I_1 = I_v$), steadiness of station setup within T ($I_2 = I_s$), uniformity of flat orography over the 2 km radius fetch ($I_3 = I_t$), uniformity of roughness over the same fetch as above ($I_4 = I_r$), anemometer height ($I_5 = I_h$), and $\mu_j \in [0, 1]$

are the corresponding weighting factors. It follows that $C = 1$ denotes a station fully compliant with WMO provisions and fully comparable REA and stat datasets, while other values are generally intended to relatively rank the stations among the selected ones. For the sake of simplicity, all weights are set $\mu_j = 1$ in the present study, i.e. all inconsistencies are considered equally important. In the following each inconsistency index is defined, and the relevant sources of discrepancy are critically exemplified.

1. *Dataset completeness.* All the selected stations have been continuously in service along the duration of the longest time series shared by all the considered REA datasets, i.e. $T = 42$ years, from Jan 1981 to Dec 2022 (see Fig. 3). All the stat datasets refer to the same constant sampling period $\Delta t_s = 1$ h. Intermediate measurements between the hourly sampled ones are discarded, if any. It follows that the maximum cardinality of each dataset is $\# = T/\Delta t_s = 368,136$. The inconsistency index for dataset completeness is defined as $I_v = (\#V_m + \#V_i)/(T/\Delta t_s)$, where $\#V_m$ and $\#V_i$ are the cardinality of missing and invalid data subsets. Normalised $\#V_m$ and $\#V_i$ for each selected station within the whole T are shown in Fig. 7(a) together with the complementary cardinality of calms $\#V_c$ and recorded speeds-over-threshold $V > V_t$. The time series of the yearly percentages of calm $\#V_{cy}$ and missing $\#V_{my}$ data are shown in Fig. 7(b,c), respectively, with some stations pointed out by filled colour circles. The occurrences of calms and missing data are uneven both over the station ensemble (Fig. 7a) and along the time series (Fig. 7b,c). In general, the percentage of calms decreases over time starting from the surprisingly high ensemble average of 40% and approaches values close to 5%, with a sudden drop at the beginning of the Nineties (Fig. 7b). Similarly, the percentage of missing data is not constant over time: the ensemble average sightly increases up to about 30% in 2000, then it drops settling to values lower than 10% (Fig. 7c). Remarkably, even if ensemble average values of both $\#V_{cy}$ and $\#V_{my}$ are reassuringly decreasing in time, the trend at some single stations do not, e.g. Bologna ($\#V_{cy}$, Fig. 7b) or Trieste ($\#V_{my}$, Fig. 7c). The general consensus in the scientific literature reviewed in the Introduction is that such uneven generalized trend of calms is not related to change in atmospheric conditions but due to modifications to the anemometer starting threshold, due e.g. to upgraded technical specifications of newly installed ones, or decreased performances within service life of old ones. Recently, Molina et al. (2021) carried out an extensive and detailed analysis of HadISD measurements over the whole Europe: they only retained as reliable stations the ones with $(\#V + \#V_c) \geq 90\%(T/\Delta t_s)$, neglecting measurements unevenness detected over time, i.e. false calms. Only 12 stations over the 21 considered herein comply with the condition above. To overcome such a limitation, and given that comparability is meant herein to assess the REA *relative* accuracy w.r.t. stats, in the present study we retain all stations, and we consider REA results corresponding to valid stat samples only. In short, the current stat continuous T is shortened from 50 to 42 years to adapt to REA time coverage, while REA single data are discarded to match stat valid samples only. It follows that $I_v = 0$ for all stations.

2. *Steady station setup within T.* The variation over time of the station setup, e.g. anemometer position, fetch roughness, local disturbances by obstacles, cannot be systematically and directly assessed for all stations because of the lack of historical information or very high resolution orthoimagery. Recent studies (e.g. Mo et al., 2015; Huang et al., 2018) indirectly detect such changes by checking the statistical stationarity of the measurement time series, under the conjecture that non stationary time series are predominantly due to station setup variations rather than to long-term climatic trends, not significantly observed for winds in Southern Europe (e.g. Dunn et al., 2019; Rapella et al., 2023). In the present study the stationarity of yearly wind speed time series is assessed via their linear regression $V_y(t) = at + b$, by analogy to Mo et al. (2015). As a result, the station setup 'degree of non-stationarity' is conjectured to be linearly proportional to the absolute value $|a|$ of the angular coefficient of the regression, and the
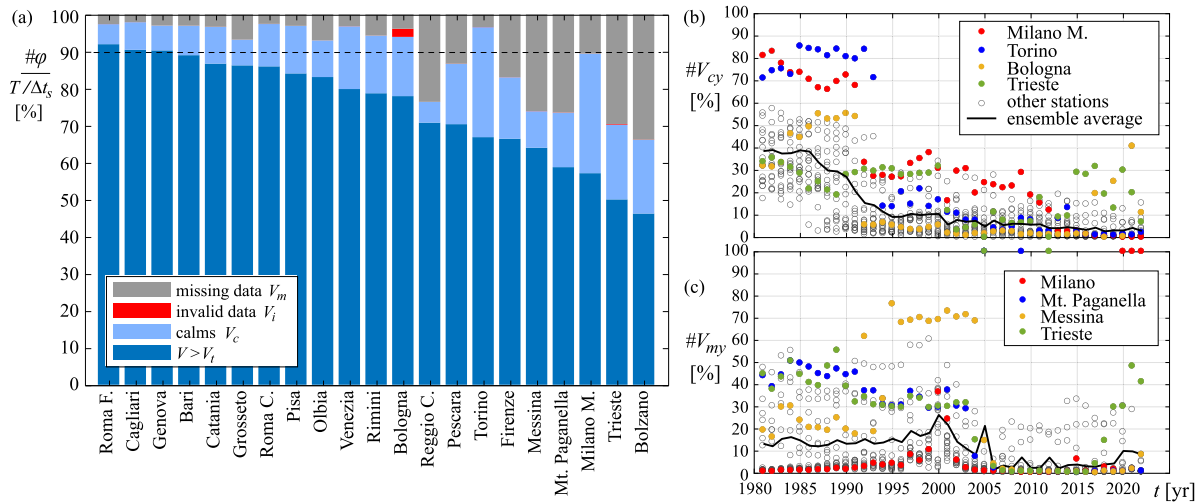
Fig. 7. Overall occurrence of missing, invalid, calm and speed-over-threshold records at the selected anemometric stations within the whole duration of the time series T (a), yearly occurrences of calm (b) and missing (c) data.

stationarity index is defined as $I_s = |a|/|\hat{a}|$, where $\hat{}$ stands for the maximum value over the ensemble of the considered stations. Please note that the index does not necessarily has the same value when referred to the current wind speed and to its annual maxima. Time series of yearly maxima $\hat{V}_y$ and yearly averages $\overline{V}_y$ wind speeds are plotted in grey in Fig. 8 for all the 21 stations. The time series of four paradigmatic stations are considered as exemplifying case studies, sorted for increasing stationarity, and pointed out in colours in separate graphs: Milano Malpensa (a,b), Cagliari Elmas (c,d), Grosseto (e,f), Venezia Tessera (g,h). The well-documented station of one of the largest and best equipped Italian airports is scrutinized in order to prove the conjectured correlation and support the argument of causation between stat setup variations and highly non stationary wind speed (Milano Malpensa, Fig. 8a,b). Historical map from Ballio et al. (1991a), more recent orthophotos of the airport layout on different years within T, and wind roses within periods around them are shown in Fig. 8(i–s). The anemometer was shifted a huge amount of times. Ballio et al. (1991a) report 6 displacements within the time interval 1956–79 (from A to F in Fig. 8i). Within 1981–91 (Fig. 8j,k), the airport was still equipped by a single anemometer, mostly exposed to open terrain conditions but with growing aerodynamic roughness and decreasing wind speed, in turn. Expansion works started at the end of 1991 to build a second terminal, then completed in 1998 (light blue interval in Fig. 8b, Hine, 1998), leading to the installation of a second anemometer. The clear discontinuous drop of $\overline{V}_y$ (Fig. 8b) is contemporary to the start of the terminal construction (Fig. 8l). Correspondingly, a switch from scattered to unimodal wind regime takes place (Fig. 8k,m), most likely induced by the new terminal buildings that locally deflect and channel the incoming flow. It is also worthwhile to note the monotonic, progressive but recently accelerated lowering of calm rate (Fig. 8k,m,o,q,s), probably induced by successive upgrade of the anemometer specifications, and reflected by the progressive increase of $\overline{V}_y$ from 2000 to 2020, in turn. The stationary series at Venezia (Fig. 8g,h), whose territory is almost exempt from urbanization or tall tree growth, further confirms in absentia the conjectured dependency between stat exposure and wind speed long term changes. On the basis of the reviewed literature and example above, wind speed non stationarity is interpreted in the following as the result of station setup variations. Overall, $\overline{V}_y$ time series (Fig. 8b,d,f,h) are more affected than $\hat{V}_y$ (Fig. 8a,c,e,g) by stat setup changes. The ensemble of the selected stations (grey points and dotted line) shows a general decreasing trend of the daily averaged wind speed, that we conjecture is overall due to the progressive increase of the roughness length induced by the growth of the urban areas in Italy (Romano et al., 2020), analogously to what reported by Mo et al. (2015) in

PRC. The selected anemometric stations in Venezia (Fig. 8g,h), Grosseto (Fig. 8e,f), Cagliari Elmas (Fig. 8c,d) and Milano Malpensa (Fig. 8a,b) are examples of almost perfectly stationary, weakly non-stationary, non-stationary and highly non-stationary time series, respectively.

3. *Uniform flatness at stat site.* The site orography index is defined as $I_t = \tilde{z}/\hat{\tilde{z}}$, where z is the elevation above the sea level, and $\tilde{}$ stands for standard deviation over the 2 km radius fetch upwind the station. Variation of orography is discussed by initially referring to three main paradigmatic setup conditions, exemplified in Fig. 9. Satellite imagery of the stat neighbourhood underlying 200 m-spaced elevation contours, 2 km radius fetch and wind roses are shown in Fig. 9(a–c). Flat terrain, e.g. at Venezia Tessera (Fig. 9a) fully meets WMO-No. 8/2021 provisions and does not affect wind regime, e.g. bimodal wind rose in the specific case. Conversely, valley or one-side concave orography, e.g. at Bolzano (Fig. 9b) channels the prevailing wind along the axis of the Adige valley, and results in a monomodal wind rose. Convex mountainous orography, e.g. the stat at the top of Mt. Paganella (Fig. 9c) results in the local wind acceleration with respect to the stations in Bolzano and Venezia, even if all the stations belong to the same climatic region (see Fig. 6). $\tilde{z}$ is evaluated over the stat-centred 2 km radius fetch by referring to the high-resolution maps from Digital Terrain Models (DTM, Tarquini et al., 2007, horizontal resolution 10 m, vertical accuracy RMSE(z) $\leq$ 3.5 m) shown in Fig. 9(d–f), together with elevation profiles along local wind directions (Fig. 9g–i). Although standard deviation is clearly not able to discriminate convex or concave orography, it is a bulk measure of the elevation changes: $\tilde{z} = \{0.6, 173, 334\}$ m at Venezia, Bolzano and Mt. Paganella, respectively.

4. *Uniform roughness at stat site.* The site roughness index is defined as $I_r = \tilde{z}_0/\hat{\tilde{z}}_0$, analogously to the orography one. Roughness variation is discussed with reference to three paradigmatic setup conditions of z_0 mapped in Fig. 10. Satellite imagery of the stat neighbourhood underlying 2 km radius fetch and wind roses are shown in Fig. 10(a–c). Homogeneous roughness, e.g. at Roma Fiumicino (Fig. 10a), fully meets WMO-No. 8/2021 provisions and does not affect wind regime, e.g. multimodal wind rose in the example. Conversely, stations at mountainous coastlines, e.g. at Genova (Fig. 10b) are subjected to sea and land winds at different yaw angles blowing over upwind fetches with very different z_0 between them. In other circumstances the aerodynamic roughness significantly varies along a single upwind direction, e.g. at Tireste lanterna (Fig. 10c), resulting in the local wind transition. $\tilde{z}_0$ is evaluated over the stat-centred 2 km radius fetch in two steps: first we refer to the satellite high-resolution maps of European land cover from CORINE inventory (CLC 2018, 2020, horizontal
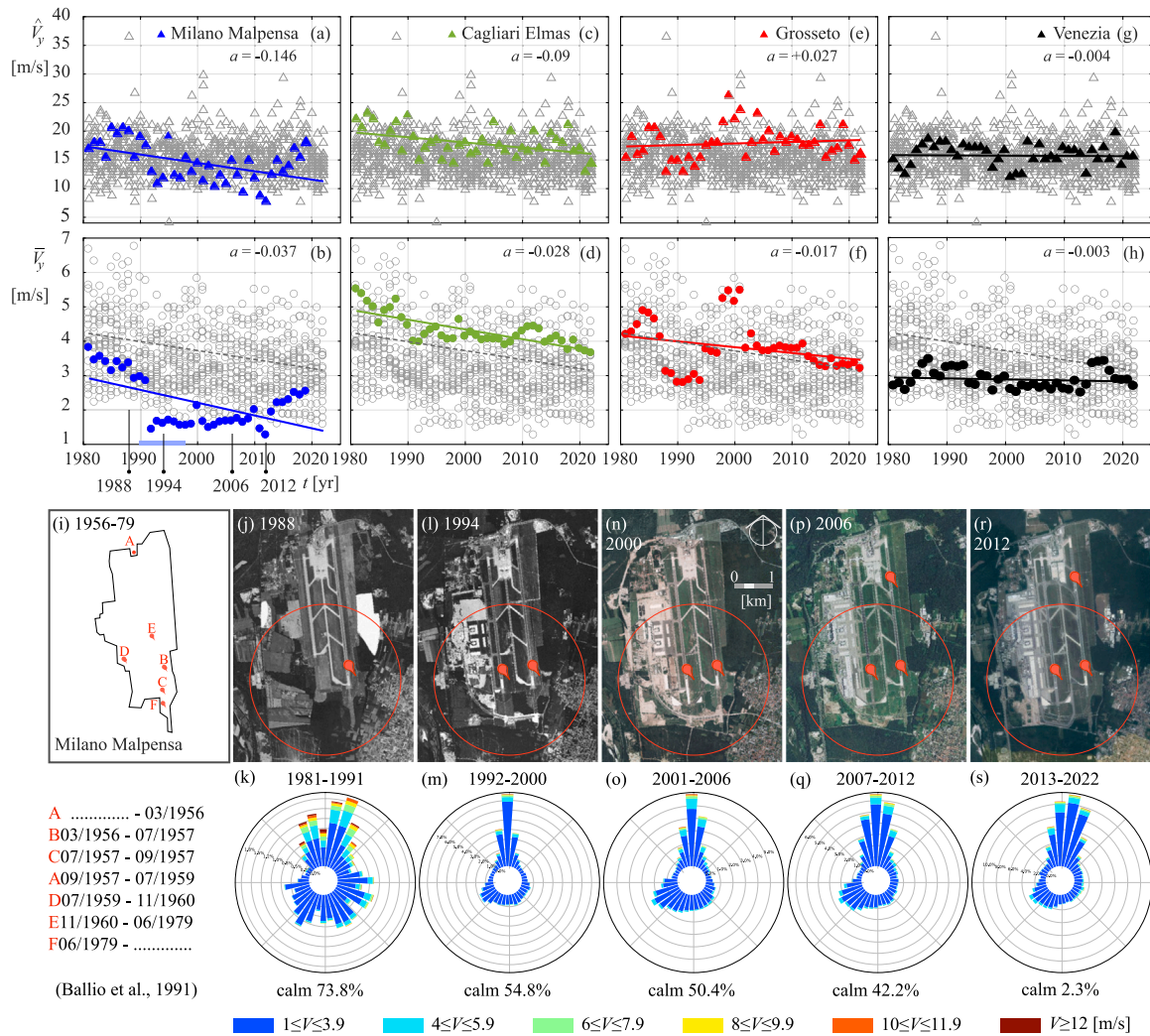
Fig. 8. Time series of the yearly maximum $\hat{V}_y$ and yearly average $\overline{V}_y$ wind speeds at Milano Malpensa (a,b), Cagliari (c,d), Grosseto (e,f), Venezia (g,h), together with underlying complete dataset (grey symbols), linear regression and its angular coefficient a. Plan view of the Milano Malpensa airport within the period [1956,1979] (i, after Ballio et al., 1991a), orthophotos (image source: www.pcn.minambiente.it) with location of the anemometer(s) (j,l,n,p,r) within the period [1988,2012], and wind roses from measurements (k,m,o,q,s) within [1981,2022].

resolution 100 m) shown by colours in Fig. 10(d–f); secondly, we establish a correspondence between the CLC 2018 44 land cover and land use classes and the EN 1991-1-4:2005 5 terrain categories, as specifically shown by patterns in Fig. 10(d–f), and generally detailed in Table A.2. The resulting z_0 profiles along local wind directions are plotted in Fig. 10(g–i): monotonic decreasing trend is observed in Genova for wind from land, while non-monotonic increasing trends occur in Genova and Trieste for sea winds. In both cases, the very uneven distributions of z_0 cross all the EN 1991-1-4:2005 roughness range in a couple of km, and are clearly due to the positioning of the anemometric stations at the interface between sea and urban fabric land cover categories. Although standard deviation is clearly not able to discriminate roughness changes along specific directions, it is a bulk measure of the overall roughness changes: $\tilde{z}_0 = \{0.0, 0.36, 0.29\}$ m at Roma Fiumicino, Genova and Trieste, respectively.

5. *Anemometer height.* None of the stations in the HadISD database have documented values of the height h of the anemometer. To the Authors' best knowledge, the same lack of data holds in other public stat measurement repositories. The 21 stations selected in this study benefit of detailed information provided in Ballio et al. (1999). The evaluation of the difference $\Delta h = h - h_{ref}$ is straightforward from Table A.1. The related inconsistency index is expressed as $I_h = |\Delta h|/|\widehat{\Delta h}|$.

In the light of the above, the compliance index in Eq. (1) is systematically evaluated for each station with $j = 2:5$ and $n = 4$. The partial inconsistency indices and the synthetic compliance ones are plotted in Fig. 11. Stations are sorted from the best performing ones (i.e. low I_j indices and high C) to the worst performing ones. Even if indices continuously vary in the range [0,1], conventional orientating watershed values are set for each index in order to discern indicative classes of consistency, i.e. the quantitative counterpart of the *'minimum requirements'* qualitatively evoked by Wieringa (1996). Concerning yearly maxima, most of the stations are classified as stationary, while only three stations are classified as non-stationary, with Milano Malpensa scoring the largest $a(\hat{V}_y)$ in absolute terms. Conversely, most of the stations are classified as weakly stationary or non-stationary concerning yearly averages, with Genova, Milano Malpensa, Bolzano and Firenze scoring the largest $a(\overline{V}_y)$ in absolute terms. Most of the stations are placed over flat or quasi-flat terrain with uniform or weakly uniform roughness. In particular, Mt. Paganella and Bolzano are confirmed as located in mountainous zones while Roma Ciampino, Trieste, Genova and Messina are placed over terrain with highly non-uniform roughness. The largest discrepancy in terms of h is attained in Trieste. In summary, 10 stations over 21 are fully WMO-compliant face to extreme winds (Venezia, Grosseto, Torino, Catania, Pisa, Reggio Calabria, Bologna, Olbia, Pescara, Roma Fiumicino, listed in decreasing order of $C(\hat{V}) \geq$
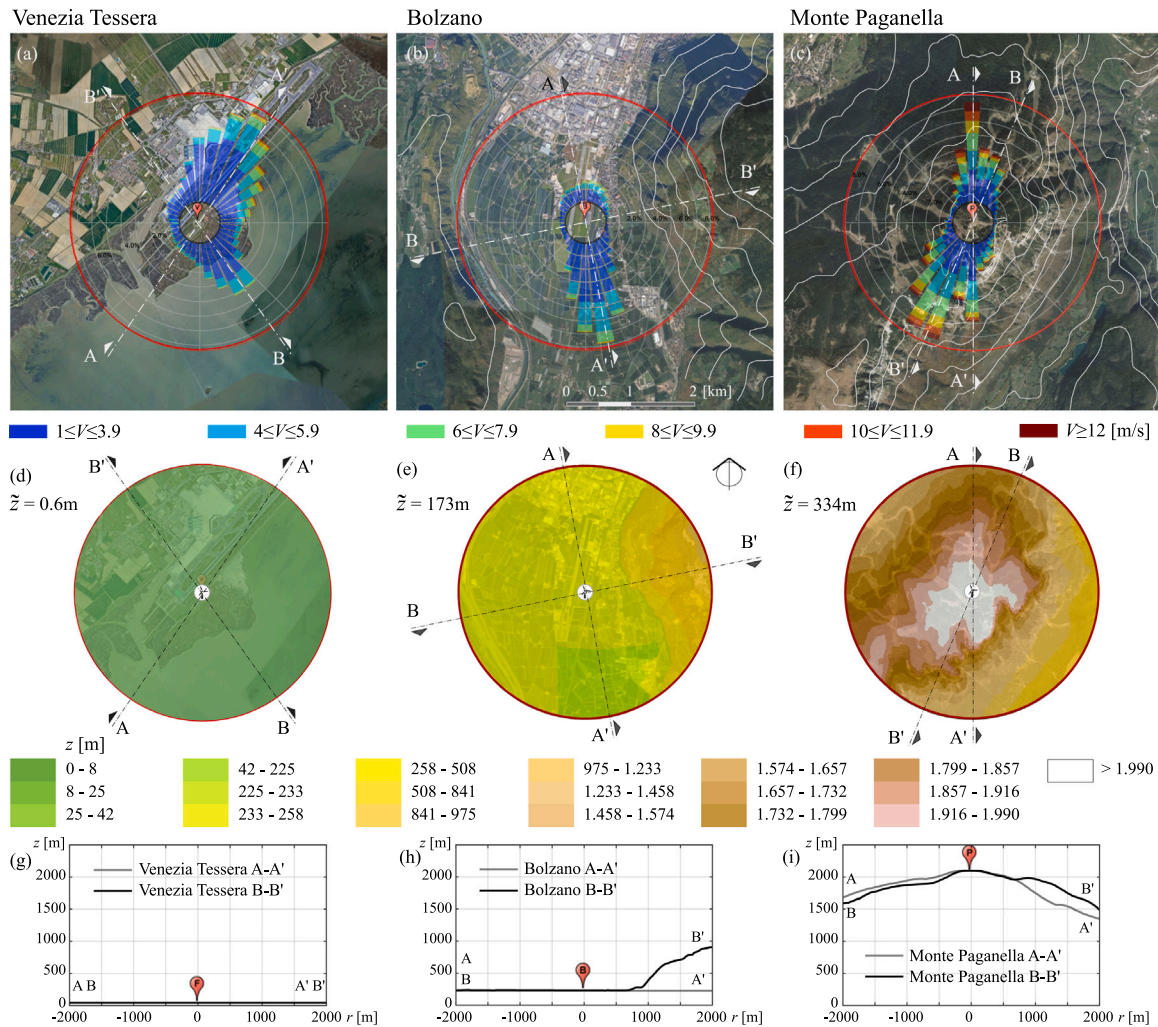
Fig. 9. Main recognized stat orographic conditions and related wind regimes: bimodal wind regime over flat terrain conditions (e.g. Venezia Tessera), monomodal wind regime along concave valley (e.g. Bolzano), bimodal wind regime over convex mountain (e.g. Mt. Paganella). For each of them: satellite imagery of the stat neighbourhood (a,b,c) underlying 200m-spaced elevation contours, 2 km radius fetch and wind rose; high-resolution map of the elevation above the sea level z from DTM over the same fetch (d,e,f); elevation profiles along prevailing wind directions (g,h,i).

0.8), while only 8/21 are also WMO-compliant face to current winds ($C(\bar{V}) \geq 0.8$, Olbia and Pescara being dropped). The measurements at the less compliant stations are significantly affected by local microscale site features, e.g. Trieste, Genova or Roma Ciampino because of sharp roughness changes, Mt. Paganella and Bolzano because of orographic effects, or Messina for both effects.

Low 'degree of compliance' stats are not a priori blacklisted in the following, but instead the stat-REA comparison will be critically discussed in the light of the stat degree of compliance. Analogously, we prefer not to transform the stat measurements by means of semi-empirical, approximated corrections (e.g. roughness-dependent geographical interpolation, Wieringa 1986, or temporally varying exposure adjustment proposed by e.g. Mo et al. 2015, Huang et al. 2018), in order not to add further approximations in the already intricate task of comparison. A single transformation is carried out on REA data in order to adjust their standard height $h_{ref} = 10$ m to the actual one of each station. The transformation adopts the classical Monin–Obukhov similarity theory (Foken, 2006) with reference to the roughness maps of each REA model (see Fig. 5).

4. Performance assessment of the REA models

In the following the performances of REA models are assessed by comparing simulation results to stat measurements. The ability of

the REA models to capture individual, real-world, phenomenologically different wind events is critically discussed first with reference to their scales in time and space. For purely illustrative purposes, two stations 300 km far apart in Northern Italy, i.e. Venezia and Milano Malpensa, are selected within the year 2018. Both stats offer high quality measurements during that time, i.e. low percentage of calms and missing data, constant exposure (see Figs. 8g,h for Venezia, 8a,b,s for Milano Malpensa). Wind speed resulting from stat measurements, ERA5, ERA5L and VHR modelling approaches are compared in Fig. 12. The whole time series of wind speed daily averages $\bar{V}_d$ are plotted in Fig. 12(a,b), while hourly speed V closeup views in correspondence of significant and well documented mesoscale events are plotted in Fig. 12(c–j).

Overall, REA datasets confirm their capability in simulating mesoscale phenomena. In general, VHR model provides the best estimate of the wind speed while ERA5/ERA5L systematically underestimate the measurements, namely during the summer, i.e. in absence of severe weather events. Individual meso-α meteorological phenomena can be clearly recognized in both time series, among them a strong Scirocco wind event (7-9 Jan, Nimbus Web, 2018b), and the renowned and destructive medicane Vaia (27-31 Oct., Nimbus Web, 2018a; Cavaleri et al., 2019). Close-up views highlight how such events are captured at both locations (Fig. 12g,h), since the distance between the two
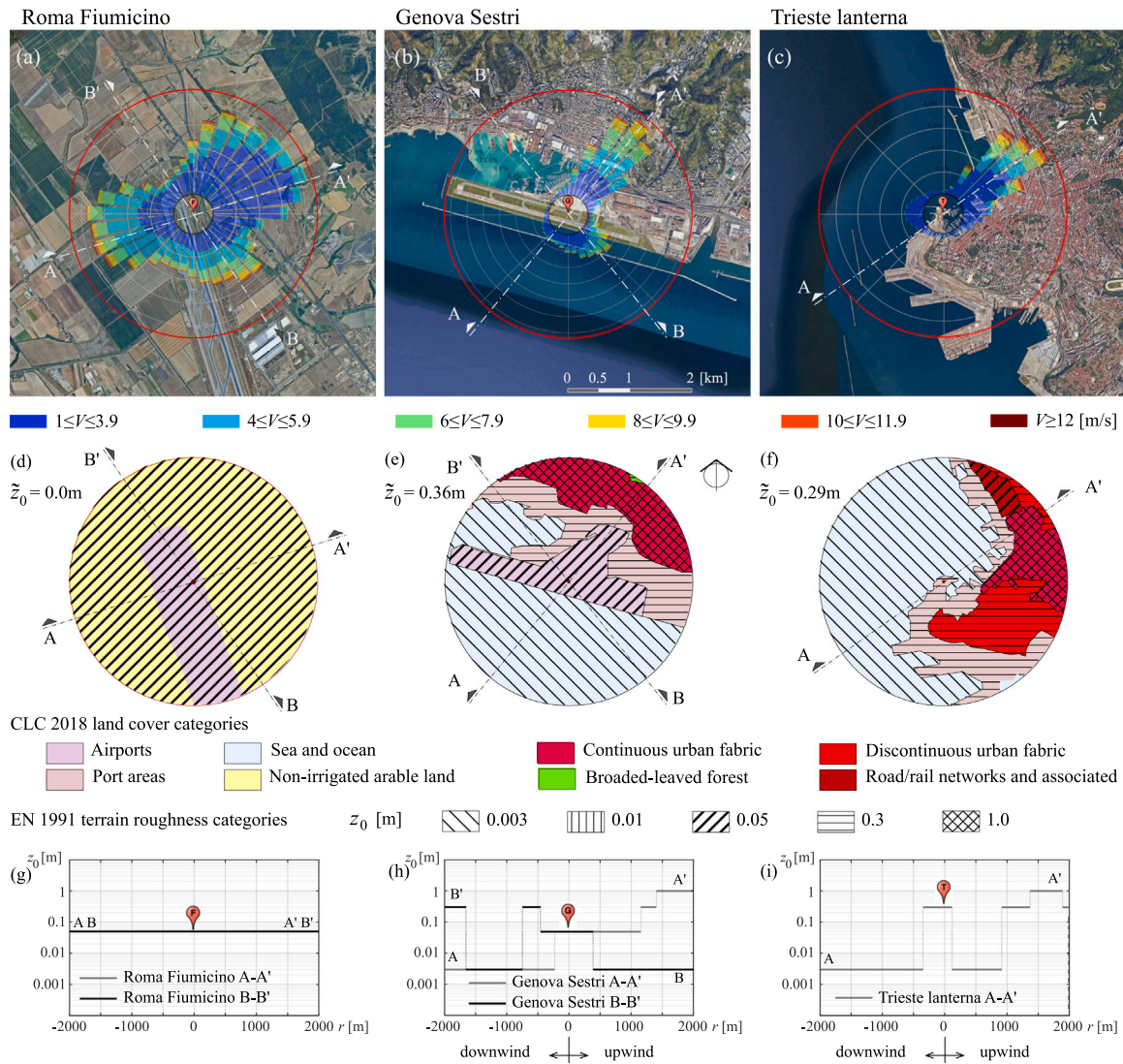
Fig. 10. Main recognized terrain covering conditions and related wind regimes: homogeneous roughness (e.g. Roma Fiumicino), nearly homogeneous roughness along each prevailing direction of the bimodal wind regime (e.g. Genova), uneven roughness along the prevailing direction of the monomodal wind regime (e.g. Trieste). For each of them: satellite imagery of the stat neighbourhood (a,b,c) underlying 2 km radius fetch and wind rose; maps of the CORINE Land Cover categories (CLC 2018, 2020, horizontal resolution 100 m) and corresponding z_0 values (after EN 1991-1-4:2005, and correspondence Table A.2) over the same fetch (d,e,f), z_0 profile along prevailing wind directions (g,h,i).

stations is in the meso-α range. Meso-β meteorological events induced by katabatic winds remain localized on the single time series, e.g. Bora wind in Feb. (a 6-day event, Nimbus Web, 2018c, Fig. 12d) and Mar. in Venezia, and North Foehn in Oct. and Dec. (Fig. 12i) in Milano. Nevertheless, REA models inevitably lead to different quantitative estimations of the wind speed magnitude. A very short duration, meso-γ thunderstorm induced by convective phenomena was reported in the evening of Mar. the 30th in Milano Malpensa inducing multiple cancelled flights (Fig. 12e, Italiavola, 2018). It appears how VHR models seem to better capture the large wind speeds induced by such kind of events. Discrepancies between VHR and the other ERA-type models result from their different horizontal resolution and modelling approaches.

In order to synthetically compare measurements and REA models over the whole considered time window T for the same two stations, the time series of wind speed yearly maxima $\widehat{V_y}$ and averages $\overline{V_y}$ are plotted in Fig. 13(a,b) for Milano Malpensa, and 13(c,d) for Venezia. Overall, ERA5 and VHR yearly maxima and averages follow the same weakly increasing trend even if they settle on two different levels, being VHR magnitudes about 1.3–1.5 times larger than ERA5 ones. However, Fig. 13(a,b) highlights that the trend of stats and REA yearly statistics

can be in strong contrast. This is also reflected in more general terms by Fig. 13(e,f) where the linear regression angular coefficients a resulting from measurements, ERA5 and VHR data obtained in correspondence of all 21 selected stations are collected. Striking differences emerge in terms of both $\overline{V_y}$ and $\widehat{V_y}$. The trends of the yearly average speed $\overline{V_y}$ (Fig. 13f) are fully stationary in REA models, while time series measured at stats are always weakly decreasing non stationary ($-0.04 < a < 0$). Whilst $\widehat{V_y}$ stat time series are mainly ranked as stationary and weakly non-stationary with decreasing trend (i.e. $-0.1 < a < 0$, Fig. 13e), ERA5 time series are ranked as stationary ($-0.05 < a < +0.05$), and VHR ones are mostly stationary with a few weakly increasing non-stationary ($+0.05 < a < +0.1$). As highlighted in Section 3, such discrepancies between measurements and REA models should be attributed to the variation over time of the terrain characteristics around anemometric stations, the presence of disturbing bodies, the shifting of the anemometer (as highlighted in e.g. Fig. 8 for Milano Malpensa), as well as replacements of the anemometer sensor. Conversely, REA models do not account for variations in exposure conditions since z_0 is mainly a time-constant parameter. In summary, stat measurements are indirectly indicative of the actual condition of the specific site exposure
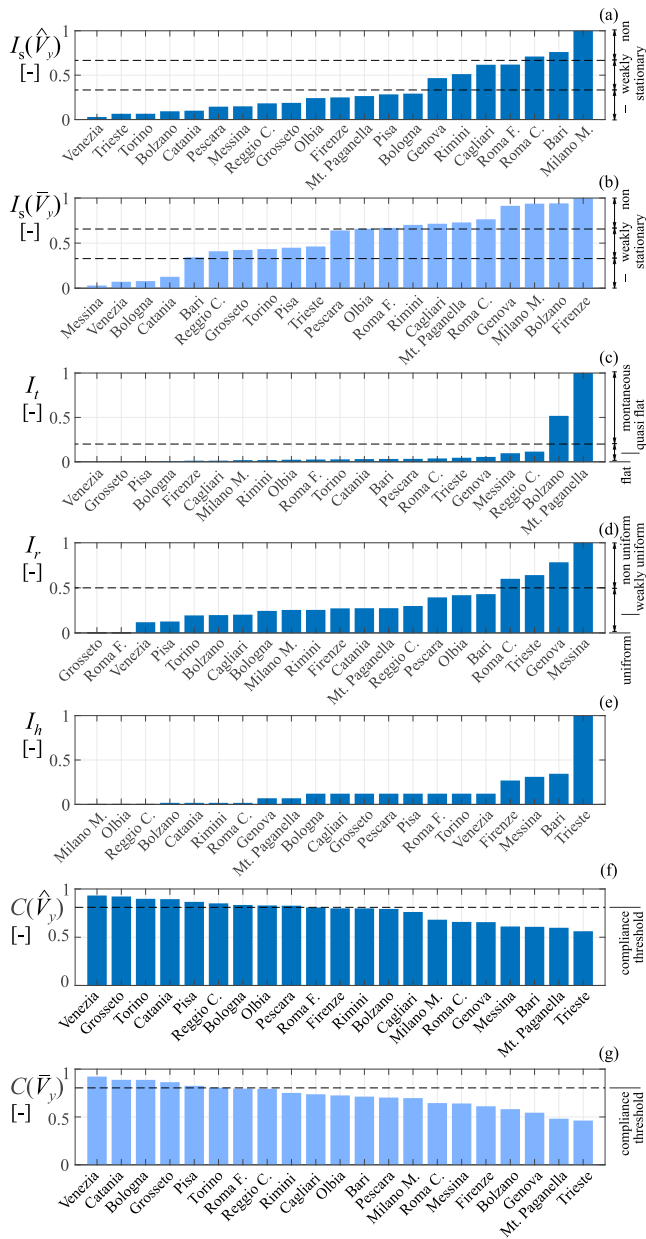
Fig. 11. Inconsistency indices related to stationarity of yearly maxima $I_s(\hat{V}_y)$ (a) and yearly averages $I_s(\overline{V}_y)$ (b), orography I_t (c), roughness I_r (d), anemometer height I_h (e). Resulting indices of compliance for yearly maxima $C(\hat{V})$ (f) and averages $C(\overline{V})$ (g).

and its changes in time, while REA models are able to rule out such changes and to point out climatic changes, if any.

The concise overall comparison between REA models and stat measurements is provided in Fig. 14. In particular, the scatter plots of mean ($\overline{V}$, Fig. 14a–c) and extreme wind speeds with 2-year (V_2, Fig. 14e–g), 50-year (V_{50}, Fig. 14i–k), 100-year (V_{100}, Fig. 14m–o), and 200-year (V_{200}, Fig. 14q–s) return periods are given. EVA POT approach is adopted to assess extreme wind speeds on both stat and REA time series to filter out uncertainty induced by statistical analysis (Torrielli et al., 2013). The POT approach fits a GPD to the exceedances over a chosen threshold. In this study, the threshold of each time series is set equal to the lowest annual maxima detected along the same time series, in agreement with Outten and Sobolowski (2021). Then, independence of extreme events is ensured by filtering extremes from consecutive events occurring within two days. In such a way, the exceedances constitute an independent identically distributed sample. From the

fitted GPD, V_{T_R} corresponds to the percentile which on average is only exceeded once within T_R. Filled and empty markers refer to WMO-compliant stations ($C(\overline{V}) \geq 0.8$ or $C(\hat{V}) \geq 0.8$) and non compliant ones, respectively. In particular, red filling colour highlights the most compliant station (Venezia), while the green, blue, and red outline colours refer to examples of non compliant stats affected by orographic changes, uneven roughness, and unsteady time series of the annual speed maxima, respectively. The REA-stat resulting relative error is expressed as:

$$\varepsilon_{REA-stat} = \frac{\phi_{REA} - \phi_{stat}}{\phi_{stat}} \qquad (2)$$

where ϕ is the generic speed statics, i.e. $\overline{V}$ and V_{T_R}. The statistics of the relative error at every selected station for each REA model are given in Fig. 14(d,h,l,p,t), in terms of box plots together with red filled and empty markers for each single compliant and non compliant station, respectively. Two very general remarks follow with reference to the whole 21 stations. First, REA models systematically predict extreme wind speeds lower than the ones measured at stats. Second, such an underestimation increases as the return period increases. With specific reference to the REA models, scatter plots resulting from ERA5 and ERA5L look qualitatively analogous, even if ERA5L errors look in average absolute value systematically slightly higher than the ones resulting from ERA5. We can conclude that the mere refined horizontal resolution obtained by interpolation in ERA5L does not improve the accuracy of the parent ERA5 wind dataset. Conversely, VHR model on the whole predicts extreme speeds closer to stat measurements, and mean speed even slightly higher than the measured ones. Convection permitting RCMs capability to more accurately simulate severe winds is also highlighted by Belušić Vozila et al. (2023) for Bora and Scirocco winds. The error is in average very small for $\overline{V}$ (Fig. 14d) and V_2 (Fig. 14h). However, the above general remarks about the stations as a whole must be enriched in more detail with specific reference to the stat degree of WMO-compliance, and related inconsistencies. First, reference to WMO-compliant station only rules out microscale effects at stations, significantly reduces the dispersion of the data, and allows to clarify the trends depicted above. For the sake of brevity, let us comment on VHR only: the mean speed is very well simulated, except for the high value in Venezia due to the very low summer wind speed $V \approx 3$ m/s (see e.g. Fig. 12b); extreme wind speed are nearly matching in Venezia, and underestimated with an error ranging from -10% to -25% for increasing T_R at the other WMO-compliant stats. Secondly, outliers and related errors up to $\pm 90\%$ can be discussed and interpreted in the light of specific stat inconsistencies. Let us bring attention to a few examples. i. The speedup at Mt. Paganella is systematically and inevitably underestimated by VHR, because of the very local orographic variation occurring at a scale smaller than the VHR horizontal resolution L (see Fig. 9i). ii. Conversely, the channelling induced by the Adige Valley at Bolzano is much better simulated by VHR than by ERA5, because L is smaller than the valley width (see Fig. 9h). iii. VHR overestimates mean and extreme speeds at stations with very uneven roughness along the wind prevailing direction(s) such as Trieste (see Fig. 10c,f,i) and Messina. iv. VHR simulates wind speed during the whole T with reference to present-day roughness length obtained by recent satellite imagery, usually higher than roughness at eighties in Italy: it follows that the VHR extreme speed are lower than the ones at stations that include old measurements obtained at low z_0 among non-stationary time series, e.g. Milano Malpensa, Roma Ciampino (see Figs. 8a and 11a). However, it is worth highlighting that the proposed compliance index has some limitations probably induced by REA model approximations, e.g. extreme wind speeds are nearly matching in Bari despite the poor compliance $C(\hat{V}_y) = 0.61$ induced by non-stationary time series, while estimates are very poor for Cagliari despite the overall fair compliance $C(\hat{V}_y) = 0.76$. In summary, ERA5 looks suitable for the estimate of the mean wind speed, despite the large dispersion of ε towards both positive and negative values. Conversely,
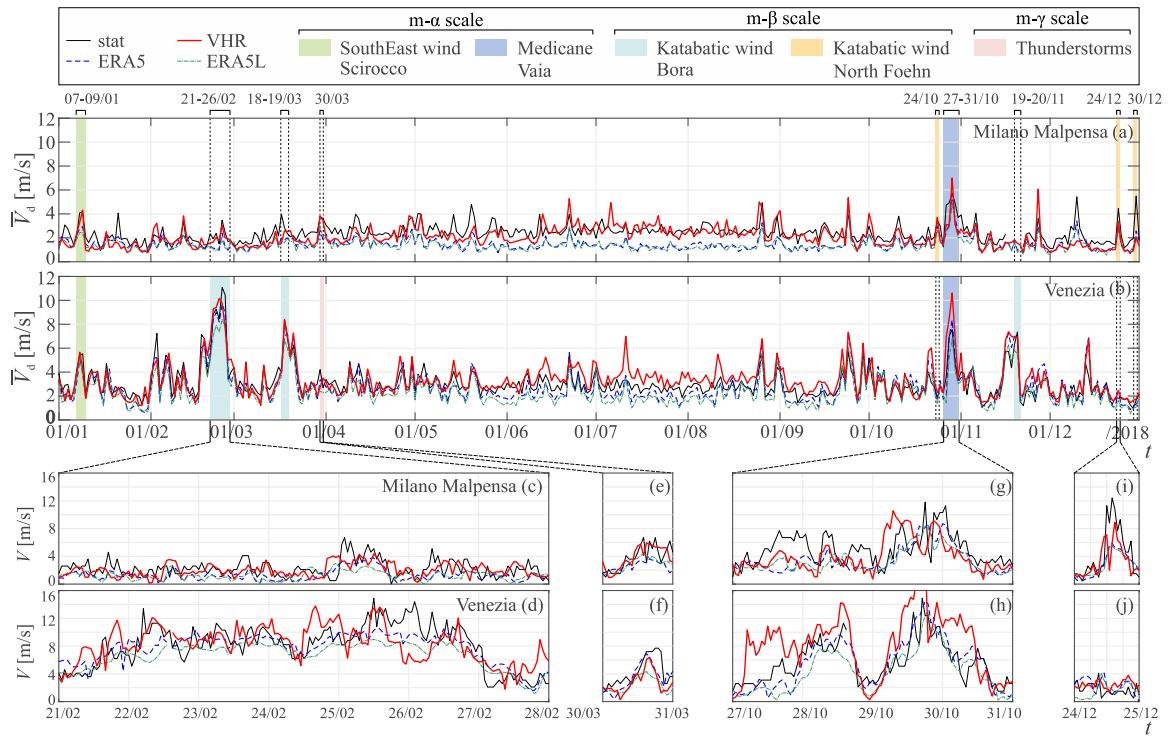
Fig. 12. Comparison among station, ERA5, ERA5L and VHR time series for Milano M. and Venezia during the year 2018: time series of daily average wind speeds $\overline{V_d}$ (a,b) and hourly wind speeds V in correspondence of individual wind events (c–j).
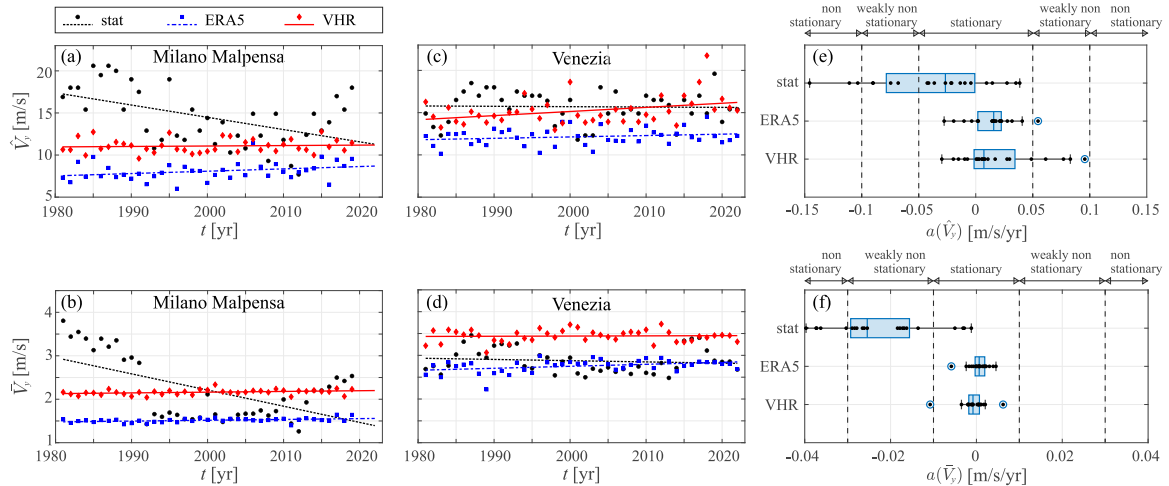

Fig. 13. Time series of yearly average $\overline{V}$ and extreme $\hat{V}$ wind speeds for Milano Malpensa (a,b) and Venezia (c,d) stations. Box plots of angular coefficients a resulting from the linear regression of $\overline{V}$ and $\hat{V}$ for measurements, ERA5 and VHR at all the selected anemometric stations (e,f).

VHR scores the lowest error in the estimation of extreme wind speeds, and it is usually associated to a shorter dispersion of ε with respect to other analysed REA models.

The VHR-based meso-γ scale Italian wind map of the extreme wind speeds is shown in Fig. 15 in terms of V_{50} filled isocontours. The other Italian maps of the mean wind speed $\overline{V}$, and extreme wind speeds V_2, V_{100}, V_{200} are provided in Annex, Fig. A.1 for the sake of brevity. As such, the drafting of each map involved the processing of about 163.5 billion wind speed data at 444,000 cells, i.e. about 160,000 times the data available 33 year ago by Ballio et al. (1991b). To better appreciate the horizontal resolution of the Italian map and its mesoscale features, a closeup isocontour view of the zone surrounding the Adige and Sarca valleys, from Bolzano to the Garda lake is shown in Fig. 15(b). The

following main considerations confirming the key features of VHR-based wind maps can be outlined: i. the spatial resolution of VHR massively enriches the description of the extreme wind speeds with respect to the current design wind speed zoning provided in the Italian standard (DM 17-01-2018, CNR-DT 207 R1/2018, Fig. 6); ii. the highest wind speed magnitudes take place over (i) water bodies, i.e. sea and lakes, due to the low roughness; and (ii) mountain ridges, due to the strong orographic effects directly accounted for. In absolute terms, the largest V_{50} in the analysed domain occurs along the Croatian coast around the Velebit mountain. Such a region has been widely recognized in the literature as an area giving rise to particularly strong Bora winds (Alpers et al., 2009; Belušić Vozila et al., 2023). Along the Italian coast, strong windy areas are recognized at the mouth of the strait of Bonifacio due to channelling effect induced by north
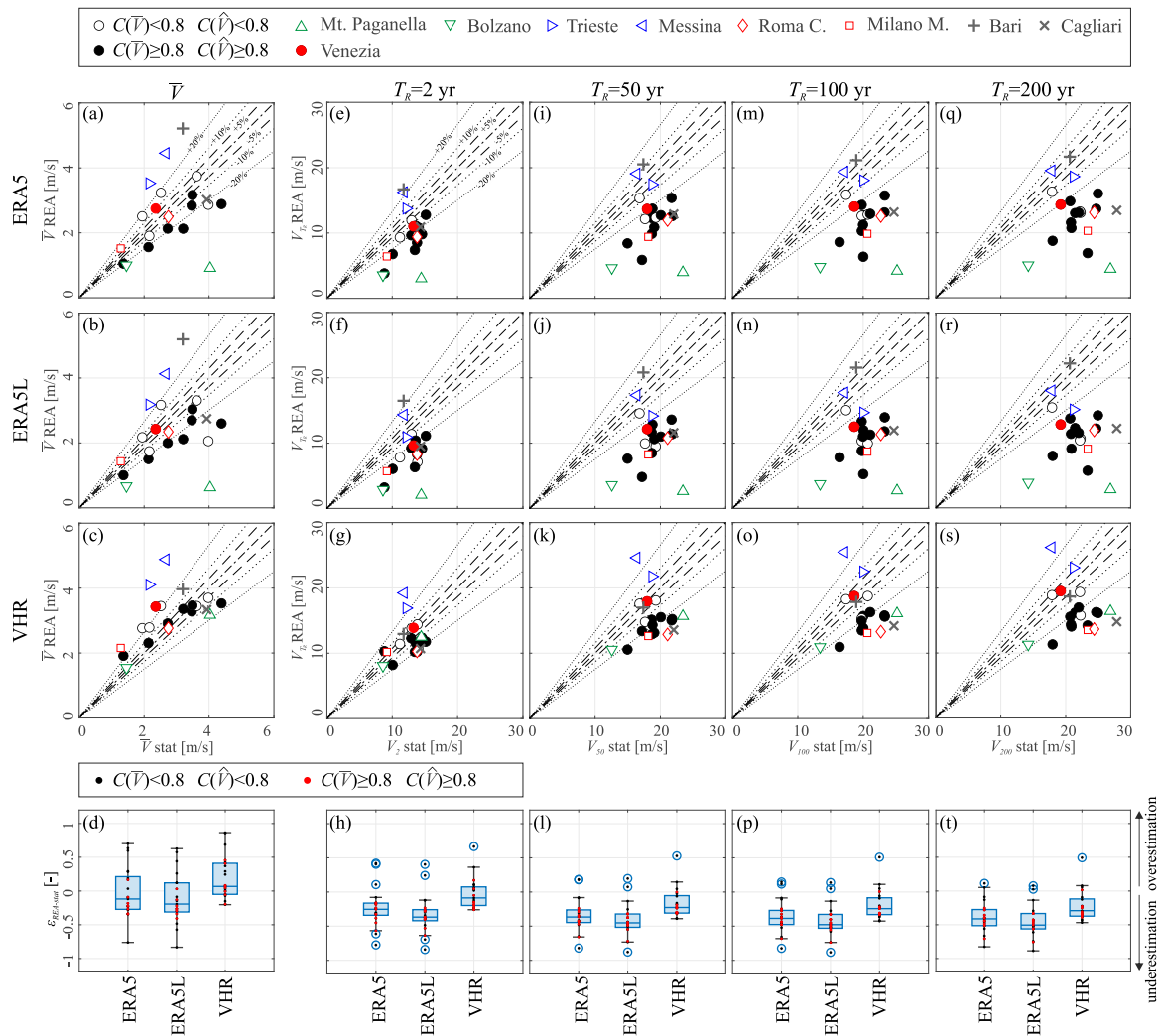
Fig. 14. Scatter plot of mean $\overline{V}$ (a–c) and extreme V_{T_R} (e–g,i–k,m–o,q–s) wind speeds resulting from REA models and stat measurements, and resulting box plots of the relative error $\varepsilon_{REA-stat}$ of REA models with respect to measurements (d,h,l,p,t).

Sardegna and south Corsica, and along the Tyrrhenian coast of Sicilia and Calabria, because of the complex orography behind the shoreline; iii. the effects induced by orography and low roughens are exemplified in the closeup view in Fig. 15(b). $V_{50} \approx 10$ m/s in proximity of Bolzano, also consistently to stat measurements. It slightly increases along the Sarca valley due to its narrowing. The microscale features of the wind speed-up at the top of Mt. Paganella are not caught, consistently with the VHR meso-γ resolution. At the mouth of Sarca valley and over the Garda lake wind speed dramatically increases, confirming the 'wind machine' reputation of the lake. Such a mesoscale speed-up is due to (i) the contribution of strong meso-β Foehn winds blowing from NorthEast and directed along the major axis of the lake (Amadori et al., 2018; Piccolroaz et al., 2019), (ii) the steep surrounding orography, and (iii) the low local roughness of the stretch of water.

5. Towards a reanalysis-based approach

The specific features and promising performances of the REA modelling approach allow us to imagine a novel *'reanalysis-and-height adjust'* (REA-HA) approach as an alternative to the in-force codified 'map-and-return' one, and as schematized in Fig. 16. The first 'reanalysis' stage including Numerical Weather Prediction, Reanalysis, Downscaling, and EVA is entrusted to the specialist in charge of drawing the map, while the 'height adjust' stage is entrusted to the designer, in analogy with the two step 'map-and-return' codified approach. The proposed approach

involves some conceptual and technical advantages with respect to the in force codified approach. At the reanalysis stage: i. forth-and-back across scales, and transformation of non-homogeneous, scattered data are no longer needed; ii. every effect including the orographic one are consistently and explicitly accounted for up to the meso-γ scale, while microscale effects are knowingly excluded; iii. the high horizontal resolution offers to the designer detailed 'maps without gaps' of the wind speed and aerodynamic roughness, including values evaluated quite close to the design site. At the height adjust stage: i. the designer is relieved of some tasks that require specialized know-how in wind engineering, namely the obligation to subjectively evaluate the aerodynamic roughness at design site, and to ascribe the actual, 3D, sometime complex site orography to simplified schemes and related orographic coefficients; ii. the designer is make conscious of what the approach accounts for, and what it does not, i.e. microscale effects of local site features inside a 2 km radius fetch. In the face of the above advantages the REA-based extreme wind speed modelling generally underestimates measurements. As such, REA-based extreme wind speed estimates shall be adjusted by means of a suitably tuned model correction factor. As a result, the design wind speed $V_m(h_d)$ is expressed in REA-HA as

$$V_m(h_d) = \gamma_m \cdot V_{REA} \cdot \frac{\ln \frac{h_d}{z_0}}{\ln \frac{h_{ref}}{z_0}}, \tag{3}$$
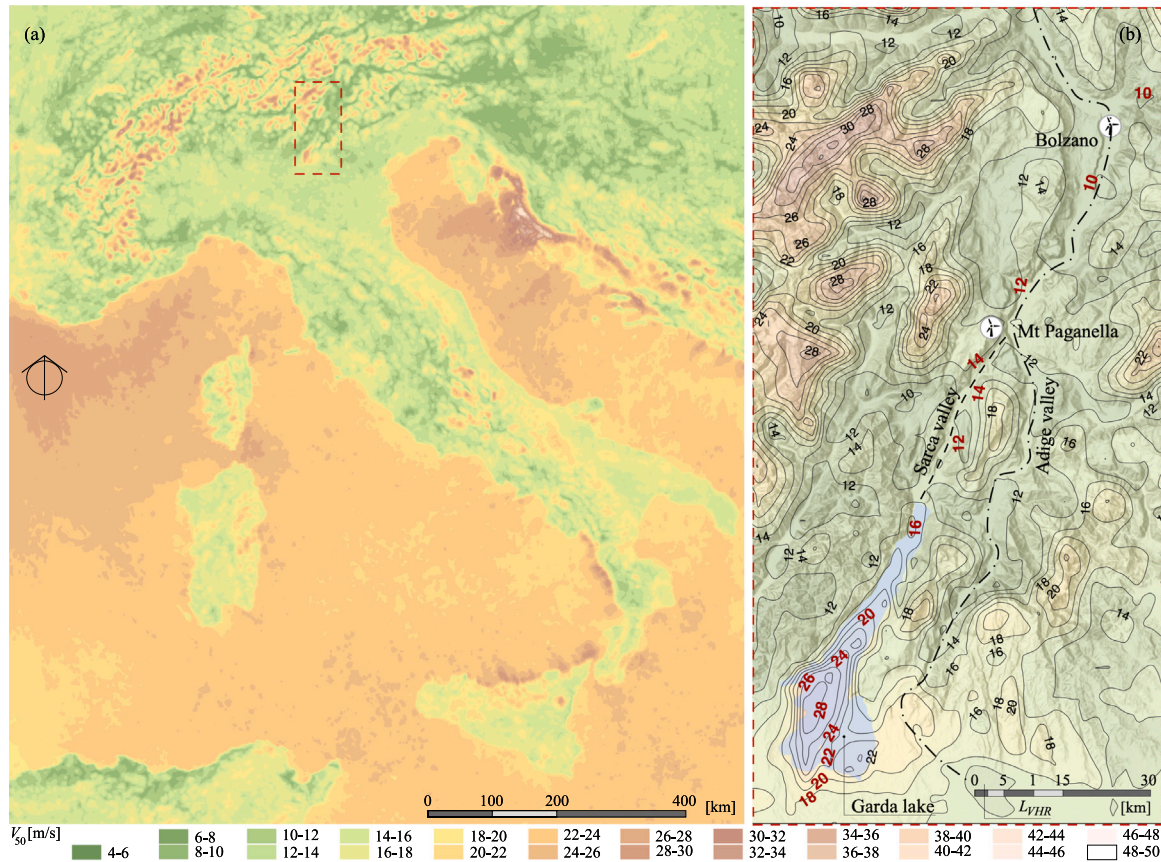
Fig. 15. Map of the extreme wind speed V_{50} with return period $T_R = 50$ in reference system ETRS89-extended/LCC Europe (a). Closeup view of the map around the zone surrounding the Adige and Sarca valleys, from Bolzano to the Garda lake (b).

where γ_m is the model correction factor, $V_{REA}(x_d, y_d)$ and $z_0(x_d, y_d)$ are the wind speed and aerodynamic roughness at the design site position (x_d, y_d) as mapped in the REA stage (e.g. in Figs. 15 and 5, respectively), h_d is the reference design height relevant to the structure under consideration, $h_{ref} = 10$ m is the reference height at which V_{REA} is mapped. In other words, the designer is only called upon to select the return period relevant to design, apply the related model correction factor γ_m and adjust the height. In the following, a first exploratory step towards the estimate of γ_m is proposed. As such, γ_m is obtained from the comparison of REA models with WMO-compliant stat measurements and results equal to:

$$\gamma_m = \frac{V_{REA}}{V_{stat}} = \frac{1}{1 + Q_2(\varepsilon_{REA-stat})} \qquad (4)$$

where $Q_2(\varepsilon_{REA-stat})$ stands for the median value of the relative error $\varepsilon_{REA-stat}$ (see Fig. 14d,h,l,p,t). γ_m shall be considered as a bulk factor accounting for REA-H approach approximations, i.e. (i) dishomogeneity of wind speed averaging periods between REA models and stat measurements (Kasperski, 2002; Picozzi et al., 2022), (ii) discrepancies in roughness length definition and values among REA models and in force standards (Yu et al., 2023), and (iii) assumption of in-equilibrium wind speed log profile (Foken, 2006) adopted in the height adjust stage in correspondence of mesoscale orographic and roughness transitions. Fig. 17 quantifies REA modelling errors by referring only to compliant stations in order to secure the representativeness of the measurements at the meso- and macro-scales, and filter out local microscale effects on wind speed.

Fig. 17(a) plots the standard deviation $\widetilde{\varepsilon}_{REA-stat}$ and median value $Q_2(\varepsilon_{REA-stat})$ of the relative error for each return period. The average constant trend of $\widetilde{\varepsilon}_{REA-stat}$ highlights how the return period does not sensibly affect the dispersion of the relative error. The exponential

decreasing trend of $Q_2(\varepsilon_{REA-stat})$ confirms the pattern qualitatively observed in Fig. 14, i.e. the systematic underestimation of the REA-based extreme wind speed with respect to station measurements for increasing return periods, with VHR and ERA5L resulting in the closest and farthest estimates to station measurements, respectively. The related values of γ_m are still provided in Fig. 17(a) by means of Eq. (4). As an example, when $T_R = 50$ yrs it results $\gamma_m = \{1.38, 1.63, 1.79\}$ for VHR, ERA5 and ERA5L, respectively. REA model deviations with respect to the codified approach (DM 17-01-2018) are shown by box plots in Fig. 17(b) particularly by referring to V_{50} estimates at compliant stations. V_{50} estimates based on DM 17-01-2018 are evaluated according to the roughness classes provided in Ballio et al. (1999). According to Fig. 17(b), DM 17-01-2018 approach results in non-negligible overestimation ranging from about 0.15 to 0.55 times station measurements. VHR-based extreme speeds result the closest ones to measurements in average terms and the least scattered, ranging from about -0.2 to -0.3 times station measurements. In light of the errors highlighted above, REA-based estimations can be corrected by means of γ_m to decrease $\varepsilon_{REA-stat}$. However, it is worth stressing that the proposed values of γ_m only take into account the modelling approximations above, while they have limited value since they neglect the uncertainties related to EVA statistical approach; they are estimated based on local observations referring to 10 stations, unevenly distributed over the Italian territory; they obviously depend on the considered REA model and have uniquely been estimated for the REA models considered in the present study; they compensate REA-based estimations in median terms only. In other words, the tuning and generalization of γ_m still deserves extensive modelling effort.
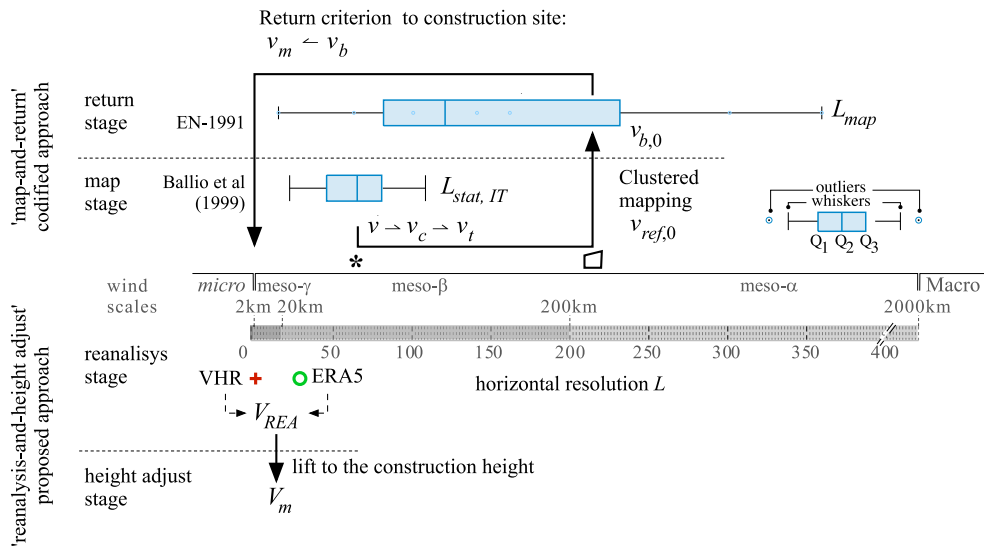
Fig. 16. Comparative workflow of the traditional 'map-and-return' approach, and of the proposed 'reanalysis-height adjust' one.
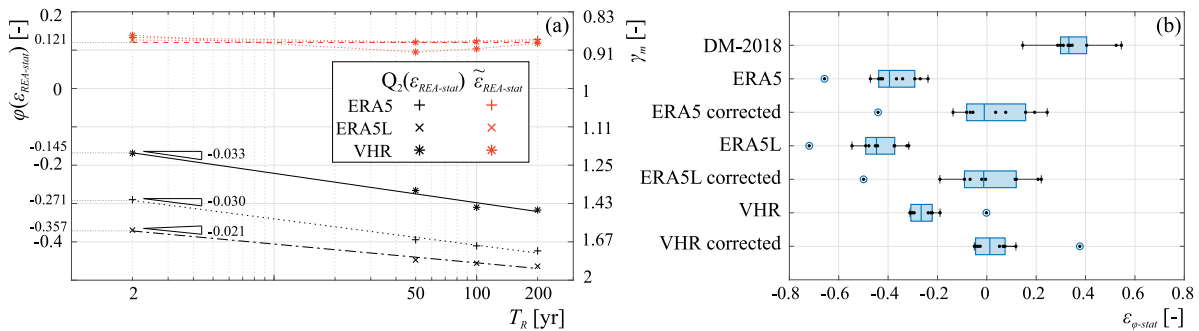

Fig. 17. Median and standard deviation of $\varepsilon_{REA-stat}$ for each model and return period at compliant stations, together with corresponding model correction factor γ_m (a). Relative errors with respect to stat measurements made on V_{50} by DM 17-01-2018 and REA models without and with model correction factor (b).

6. Conclusions and perspectives

The present study is the first effort to map the extreme wind speeds at the lower bound of the meso-γ scale resolution over the whole Italian territory. Three different reanalysis-based models are adopted, described and discussed in the light of their strengths and weaknesses face to Wind Engineering problems. 21 anemometric stations over the Italian territory are selected for comparison, and their compliance to WMO specification quantitatively assessed by means of a novel synthetic index. The performances of REA models are critically compared with measurements. Mesoscale maps of mean and extreme wind speeds with 2, 50, 100, and 200-year return periods are given. Finally, a new engineering REA-HA approach to the definition of the design wind speed is proposed. This study suggests that mesoscale wind maps are a promising tool for engineers and designers, provided that a correction factor covering modelling approximations is applied.

The proposal of a novel reanalysis-based approach to mesoscale wind maps opens the door to a number of research and applications perspectives. Research perspectives are intended to improve the proposed approach for design and assessment engineering purposes. Among them, we mention:

- the critical comparison of the performances of different global and regional models in drafting extreme wind maps in general, and in simulating meso-γ scale winds such as thunderstorms in particular;
- the correction of the 'reanalysis-and-height adjust' approach current approximations by accounting for the different averaging period in VHR (Picozzi et al., 2022), and wind speed transition profile in correspondence of mesoscale orographic and roughness transitions;
- the improvement of the proposed model correction factor to account for further modelling uncertainties.

Application perspectives are intended to directly exploit the proposed approach and obtained results. Some of them are mentioned in the following, necessarily not exhaustive list:

- the same approach would allow to draw a unified European map of extreme winds to overcome the inconsistencies among the national maps at their administrative borders, as pointed out by Miller (2003) and Ricciardelli (2023). The ongoing Euro-CORDEX dynamical downscaling at European region wide level (Jacob et al., 2020) offers a real prospect (Outten and Sobolowski, 2021) towards such an ambitious project;
- mesoscale wind maps considering the effect of climate change can be drawn to predict extreme wind scenarios and their impact on both built and natural environment (e.g. Raffa et al., 2023);
- specific mesoscale maps can be drawn for line-like infrastructures such as railways (Burlando et al., 2010; Freda and Solari, 2010; Gageik et al., 2024), highways, power lines (Yang et al., 2022);
- coupling the mesoscale maps with microscale CWE simulations (see e.g. Bruno et al., 2023, Fig. 11) or wind tunnel tests at point-wise locations to account for local effects of orography, roughness transition, large man-built obstacles, if deemed useful by the designer in the light of the specific features of the construction site and of the structure.

Table A.1

Main data of the 21 Italian stations selected for model comparison: latitude and longitude in WGS84, elevation above the sea level z, anemometer height h after Ballio et al. (1999), #V after HadISD database (Dunn et al., 2016), z_0 values according to Ballio et al. (1999) and adopted in DM 17-01-2018, CNR-DT 207 R1/2018.

WMO ID	Name	lat [°N]	lon [°E]	z [m]	h [m]	#$V/(T/\Delta t)$ [%]	z_0 [m]
162700	Bari Palese	41.136815	16.750374	53.9	20.0	96.9%	0.05
161400	Bologna	44.533595	11.297869	37.5	6.5	93.9%	0.05
160200	Bolzano	46.456408	11.32818	240.5	10.5	66.1%	0.10
165600	Cagliari Elmas	39.243436	9.061239	4.0	6.5	97.9%	0.05
164600	Catania Fontanarossa	37.464628	15.058334	11.9	10.5	96.6%	0.05
161700	Firenze Peretola	43.808494	11.200437	43.9	17.8	82.9%	0.05
161200	Genova Sestri	44.412199	8.846559	4.0	8.0	96.9%	0.10
162060	Grosseto	42.753149	11.062691	4.6	6.5	93.1%	0.05
160660	Milano Malpensa	45.617316	8.728465	233.8	10.0	89.4%	0.05
164200	Messina torre faro	38.19659	15.562812	51.0	19.0	73.8%	0.30
160220	Monte Paganella	46.143434	11.037547	2129	12.0	73.4%	0.30
165310	Olbia Costa Smeralda	40.896075	9.509907	11.3	10.0	92.9%	0.05
162300	Pescara	42.436981	14.186816	14.6	6.5	86.6%	0.05
161580	Pisa	43.675693	10.388302	1.8	6.5	96.9%	0.05
164220	Reggio Calabria	38.072677	15.654654	29.3	10.0	76.3%	0.05
161490	Rimini	44.016655	12.621431	12.5	10.5	94.2%	0.05
162390	Roma Ciampino	41.805313	12.589321	130.1	10.5	97.3%	0.05
162420	Roma Fiumicino	41.843467	12.264466	4.6	6.5	97.3%	0.05
160590	Torino Caselle	45.191654	7.650843	301.4	6.5	96.5%	0.05
161100	Trieste lanterna	45.649228	13.755992	20.0	39.0	70.2%	0.10
161050	Venezia Tessera	45.495304	12.34173	2.1	6.5	96.8%	0.05

CRediT authorship contribution statement

Lorenzo Raffaele: Writing – review & editing, Writing – original draft, Visualization, Validation, Methodology, Investigation, Formal analysis, Data curation, Conceptualization. **Luca Bruno:** Writing – review & editing, Writing – original draft, Visualization, Supervision, Methodology, Investigation, Funding acquisition, Formal analysis, Conceptualization. **Elisabetta Colucci:** Writing – review & editing, Writing – original draft, Visualization, Data curation.

Declaration of competing interest

The authors declare that they have no known competing financial interests or personal relationships that could have appeared to influence the work reported in this paper.

Data availability

The wind maps in Fig. 15 and Figs. A.1 are browsable and zoomable over the whole Italian Country in Open Access at https://arcg.is/1jzizj1 and https://geowindy.polito.it/projects/.

Acknowledgements

Appendix

See Tables A.1 and A.2 and Fig. A.1

Table A.2

Correspondence table between CLC 2018 classes and EN 1991-1-4:2005 terrain categories.

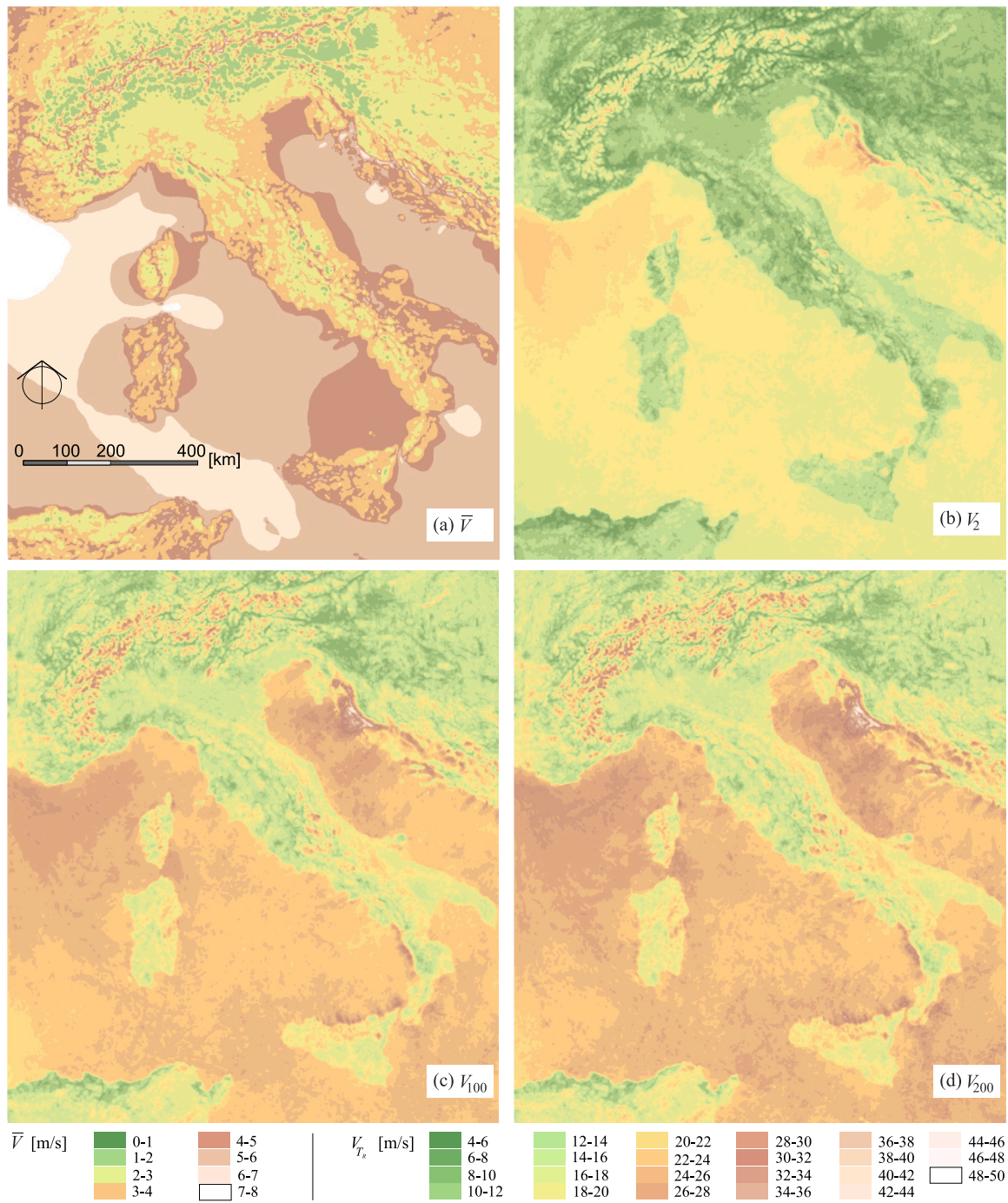| CORINE Land Cover (CLC 2018)		EN 1991-1-4:2005	
Class nb.	Class name	z_0 terrain cat.	z_0 [m]
111	Continuous urban fabric	4	1
112	Discontinuous urban fabric	3	0.3
121	Industrial or commercial units	3	0.3
122	Road and rail networks and associated land	2	0.05
123	Port areas	3	0.3
124	Airports	2	0.05
131	Mineral extraction sites	2	0.05
132	Dump sites	2	0.05
133	Construction sites	2	0.05
141	Green urban areas	2	0.05
142	Sport and leisure facilities	2	0.05
211	Non-irrigated arable land	2	0.05
212	Permanently irrigated land	2	0.05
213	Rice fields	2	0.05
221	Vineyards	2	0.05
222	Fruit trees and berry plantations	3	0.3
223	Olive groves	3	0.3
231	Pastures	2	0.05
241	Annual crops associated with permanent crops	2	0.05
242	Complex cultivation patterns	2	0.05
243	Land principally occupied by agriculture	2	0.05
244	Agro-forestry areas	3	0.3
311	Broad-leaved forest	3	0.3
312	Coniferous forest	3	0.3
313	Mixed forest	3	0.3
321	Natural grassland	2	0.05

(continued on next page)

Fig. A.1. Map of the average value of the current wind speed (a), maps of the extreme wind speed with return period $T_R = 2$ (b), $T_R = 100$ (c), $T_R = 200$ (d) yr.

Table A.2 (*continued*).

CORINE Land Cover (CLC 2018)		EN 1991-1-4:2005	
Class nb.	Class name	z_0 terrain cat.	z_0 [m]
322	Moors and heathland	2	0.05
323	Sclerophyllous vegetation	2	0.05
324	Transitional woodland/shrub	2	0.05
331	Beaches, dunes, sands	1	0.01
332	Bare rock	1	0.01
333	Sparsely vegetated areas	2	0.05
334	Burnt areas	2	0.05
335	Glaciers and perpetual snow	1	0.01
411	Inland marshes	2	0.05
412	Peatbogs	1	0.01

Table A.2 (*continued*).

CORINE Land Cover (CLC 2018)		EN 1991-1-4:2005	
Class nb.	Class name	z_0 terrain cat.	z_0 [m]
421	Salt marshes	1	0.01
422	Salines	1	0.01
423	Intertidal flats	1	0.01
511	Water courses	1	0.01
512	Water bodies	1	0.01
521	Coastal lagoons	0	0.003
522	Estuaries	0	0.003
523	Sea and ocean	0	0.003

References

Adinolfi, M., Raffa, M., Reder, A., Mercogliano, P., 2023. Investigation on potential and limitations of ERA5 reanalysis downscaled on Italy by a convection-permitting model. Clim. Dyn. 61, 4319–4342. http://dx.doi.org/10.1007/s00382-023-06803-w.

Almendra-Martín, L., Martínez-Fernández, J., González-Zamora, A., Benito-Verdugo, P., Herrero-Jiménez, C.M., 2021. Agricultural drought trends on the iberian peninsula: An analysis using modeled and reanalysis soil moisture products. Atmosphere 12. http://dx.doi.org/10.3390/atmos12020236.

Alpers, W., Ivanov, A., Horstmann, J., 2009. Observations of bora events over the Adriatic Sea and Black Sea by spaceborne synthetic aperture radar. Mon. Weather Rev. 137, 1150–1161. http://dx.doi.org/10.1175/2008MWR2563.1.

Amadori, M., Piccolroaz, S., Giovannini, L., Zardi, D., Toffolon, M., 2018. Wind variability and earth's rotation as drivers of transport in a deep, elongated subalpine lake: The case of Lake Garda. J. Limnol. 77. http://dx.doi.org/10.4081/jlimnol.2018.1814.

AS/NZS 1170.2:2021, 2021. Australian / New Zeland Standard - Structural Design Actions, Part 2: Wind Actions. Standard, Standards New Zealand, Auckland, New Zeland.

Azorin-Molina, C., Pirooz, A.A.S., Bedoya-Valestt, S., Utrabo-Carazo, E., Andres-Martín, M., Shen, C., Minola, L., Guijarro, J.A., Aguilar, E., Brunet, M., Flay, R.G., Vicente-Serrano, S.M., McVicar, T.R., Chen, D., 2023. Biases in wind speed measurements due to anemometer changes. Atmos. Res. 289, 106771. http://dx.doi.org/10.1016/j.atmosres.2023.106771.

Ballio, G., Lagomarsino, S., Piccardo, G., Solari, G., 1991a. A first step towards the map of Italian extreme winds. Part 1 : General principles and analysis methodology. Costruzioni Metall. 3, 147–172.

Ballio, G., Lagomarsino, S., Piccardo, G., Solari, G., 1991b. A first step towards the map of Italian extreme winds. Part 2 : Results, repercussion on standards, design implications. Costruzioni Metall. 4, 209–242.

Ballio, G., Lagomarsino, S., Piccardo, G., Solari, G., 1996. La nuova mappa dei venti estremi Italiani (the new extreme wind Italian map). pp. 147–181, (in Italian).

Ballio, G., Lagomarsino, S., Piccardo, G., Solari, G., 1999. Probabilistic analysis of Italian extreme winds: Reference velocity and return criterion. Wind Struct. 2, 51–68. http://dx.doi.org/10.12989/was.1999.2.1.051.

Bartholomé, E., Belward, A., 2005. GLC2000: A new approach to global land cover mapping from earth observation data. Int. J. Remote Sens. 26, 1959–1977. http://dx.doi.org/10.1080/01431160412331291297.

Belušić Vozila, A., Belušić, D., Telišman Prtenjak, M., Güttler, I., Bastin, S., Brisson, E., Demory, M.E., Dobler, A., Feldmann, H., Hodnebrog, Ø., Kartsios, S., Keuler, K., Lorenz, T., Milovac, J., Pichelli, E., Raffa, M., Soares, P.M.M., Tölle, M.H., Truhetz, H., de Vries, H., Warrach-Sagi, K., 2023. Evaluation of the near-surface wind field over the Adriatic region: local wind characteristics in the convection-permitting model ensemble. Clim. Dyn. 61, 4319–4342. http://dx.doi.org/10.1007/s00382-023-06703-z.

Bruno, L., Coste, N., Mannini, C., Mariotti, A., Patruno, L., Schito, P., Vairo, G., 2023. Codes and standards on computational wind engineering for structural design: State of art and recent trends. Wind Struct. 37, 133–151. http://dx.doi.org/10.12989/was.2023.37.2.133.

Burlando, M., Freda, A., Ratto, C., Solari, G., 2010. A pilot study of the wind speed along the Rome–Naples HS/HC railway line. Part 1-numerical modelling and wind simulations. J. Wind Eng. Ind. Aerodyn. 98, 392–403. http://dx.doi.org/10.1016/j.jweia.2009.12.006.

Cavaleri, L., Bajo, M., Barbariol, F., Bastianini, M., Benetazzo, A., Bertotti, L., Chiggiato, J., Davolio, S., Ferrarin, C., Magnusson, L., Papa, A., Pezzutto, P., Pomaro, A., Umgiesser, G., 2019. The october 29, 2018 storm in northern Italy - An exceptional event and its modeling. Prog. Oceanogr. 178, 102178. http://dx.doi.org/10.1016/j.pocean.2019.102178.

Chiodi, R., Ricciardelli, F., 2014. Three issues concerning the statistics of mean and extreme wind speeds. J. Wind Eng. Ind. Aerodyn. 125, 156–167. http://dx.doi.org/10.1016/j.jweia.2013.12.009.

CLC 2018, 2020. CORINE Land Cover 2018 (Vector), Europe, 6-Yearly - Version 2020 20u1, May 2020. Technical Report, URL: https://land.copernicus.eu/en/products/corine-land-cover/clc2018.

CNR-DT 207 R1/2018, 2018. Guide for the Assessment of Wind Actions and Effects on Structures. Standard, National Research Council (CNR), Rome, Italy.

Cook, N., Prior, M., 1987. Extreme wind climate of the United Kingdom. J. Wind Eng. Ind. Aerodyn. 26, 371–389. http://dx.doi.org/10.1016/0167-6105(87)90006-7.

Davenport, A., 1960. Rationale for determining design wind velocities. J. Struct. Div. 86, 39–68. http://dx.doi.org/10.1061/JSDEAG.00005.

Davenport, A., 1961. A Statistical Approach to the Treatment of Wind Loading on Tall Masts and Suspension Bridges (Ph.D. thesis). Department of Civil Engineering, University of Bristol, United Kingdom.

Davenport, A., 1965. The relationship of wind structure to wind loading. In: Proceedings of the Conference on Wind Effects on Structures, NPL, 1965. ICWE-1, Vol. 1965, HMSO, pp. 53–102.

DM 17-01-2018, 2018. Technical Standards for Construction - Update DM January 17, 2018. Standard, Ministry of Infrastructures and Transport, Rome, Italy.

Do, H.X., Westra, S., Leonard, M., Gudmundsson, L., 2020. Global-scale prediction of flood timing using atmospheric reanalysis. Water Resour. Res. 56, e2019WR024945. http://dx.doi.org/10.1029/2019WR024945.

Doddy Clarke, E., Griffin, S., McDermott, F., Monteiro Correia, J.a., Sweeney, C., 2021. Which reanalysis dataset should we use for renewable energy analysis in Ireland? Atmosphere 12. http://dx.doi.org/10.3390/atmos12050624.

Dolman, A., 1986. Estimates of roughness length and zero plane displacement for a foliated and non-foliated oak canopy. Agricult. Forest. Meterol. 36, 241–248. http://dx.doi.org/10.1016/0168-1923(86)90038-9.

Doms, G., Baldauf, M., 2013. A Description of the Nonhydrostatic Regional COSMO-Model. Part I: Dynamics and Numerics. Technical Report, http://dx.doi.org/10.5676/DWD_pub/nwv/cosmo-doc_5.00_I, Consortium for Small-Scale Modelling.

Doms, G., Forstner, J., Heise, E., Herzog, H., Mironov, D., Raschendorfer, M., Reinhardt, T., Ritter, B., Schrodin, R., Schulz, J., Vogel, G., 2013. A Description of the Nonhydrostatic Regional COSMO-Model. Part II: Physical Parametrizations. Technical Report, http://dx.doi.org/10.5676/DWD_pub/nwv/cosmo-doc_5.00_II, Consortium for Small-Scale Modelling.

Dunn, R., 2019. Hadisd Version 3: Monthly Updates. Technical Report, Technical Note, no. 103, Met Office Hadley Centre.

Dunn, R.J.H., Willett, K.M., Parker, D.E., 2019. Changes in statistical distributions of sub-daily surface temperatures and wind speed. Earth Syst. Dyn. 10, 765–788. http://dx.doi.org/10.5194/esd-10-765-2019.

Dunn, R.J.H., Willett, K.M., Parker, D.E., Mitchell, L., 2016. Expanding HadISD: quality-controlled, sub-daily station data from 1931. Geosci. Instrum. Methods Data Syst. 5, 473–491. http://dx.doi.org/10.5194/gi-5-473-2016.

Dunn, R.J.H., Willett, K.M., Thorne, P.W., Woolley, E.V., Durre, I., Dai, A., Parker, D.E., Vose, R.S., 2012. Hadisd: a quality-controlled global synoptic report database for selected variables at long-term stations from 1973–2011. Clim. Past 8, 1649–1679. http://dx.doi.org/10.5194/cp-8-1649-2012.

Dyrbye, C., Hansen, S., 1996. Wind Loads on Structures. Wiley.

ECMWF, 2016a. IFS Documentation CY41R2 - Part III: Dynamics and Numerical Procedures. ECMWF, p. 3. http://dx.doi.org/10.21957/83wouv80.

ECMWF, 2016b. IFS Documentation CY41R2 - Part IV: Physical Processes. ECMWF, p. 4. http://dx.doi.org/10.21957/tr5rv27xu.

EN 1991-1-4:2005, 2005. Eurocode 1 – Actions on Structures – Part 1-4: General Actions – Wind Actions. Standard, European Committee for Standardization (CEN), Brussels, Belgium.

Foken, T., 2006. 50 Years of the Monin–Obukhov similarity theory. Bound.-Layer Meteorol. 119, 431–447. http://dx.doi.org/10.1007/s10546-006-9048-6.

Freda, A., Solari, G., 2010. A pilot study of the wind speed along the Rome–Naples HS/HC railway line. Part 2-probabilistic analyses and methodology assessment. J. Wind Eng. Ind. Aerodyn. 98, 404–416. http://dx.doi.org/10.1016/j.jweia.2009.12.005.

Fujita, T.T., 1986. Mesoscale Classifications: Their History and their Application to Forecasting. American Meteorological Society, Boston, MA, pp. 18–35. http://dx.doi.org/10.1007/978-1-935704-20-1_2.

Gageik, M., Rodriguez Ahlert, C.J., Coste, N., Raffaele, L., 2024. A multi-scale gap-bridging cwe approach to windblown sand action on critical infrastructures: Modelling framework and case study on a high-speed railway line. J. Wind Eng. Ind. Aerodyn. 249, 105722. http://dx.doi.org/10.1016/j.jweia.2024.105722.

Gesualdo, G.C., Benso, M.R., Sass, K.S., Mendiondo, E.M., 2024. Index-based insurance to mitigate current and future extreme events financial losses for water utilities. Int. J. Disaster Risk Reduct. 100, 104218. http://dx.doi.org/10.1016/j.ijdrr.2023.104218.

Gibson, J., Kållberg, P., Uppala, S., Hernandez, A., Nomura, A., Serrano, E., 1997. ERA Description. Shinfield Park, Reading.

Gomes, M.I., Guillou, A., 2015. Extreme value theory and statistics of univariate extremes: A review. Internat. Statist. Rev. 83, 263–292. http://dx.doi.org/10.1111/insr.12058.

Grimmond, C.S.B., Oke, T.R., 1999. Aerodynamic properties of urban areas derived from analysis of surface form. J. Appl. Meteorol. 38, 1262–1292. http://dx.doi.org/10.1175/1520-0450(1999)038<1262:APOUAD>2.0.CO;2.

Gualtieri, G., 2021. Reliability of ERA5 reanalysis data for wind resource assessment: A comparison against tall towers. Energies 14. http://dx.doi.org/10.3390/en14144169.

Gualtieri, G., 2022. Analysing the uncertainties of reanalysis data used for wind resource assessment: A critical review. Renew. Sustain. Energy Rev. 167. http://dx.doi.org/10.1016/j.rser.2022.112741.

Gumuscu, I., Islek, F., Yuksel, Y., Sahin, C., 2023. Spatiotemporal long-term wind and storm characteristics over the eastern mediterranean sea. Reg. Stud. Mar. Sci. 63, 102996. http://dx.doi.org/10.1016/j.rsma.2023.102996.

Hartkamp, A.D., De Beurs, K., Stein, A., White, J.W., 1999. Interpolation Techniques for Climate Variables. NRG-GIS Series 99-01, CIMMYT, Mexico, D.F.

Hastings, D., Dumbar, P., Elphingstone, G., Bootz, M., Murakami, H., Maruyama, H., Masaharu, H., Holland, P., Payne, J., Bryant, N., Logan, T., Murre, J., Schreier, G., MacDonald, J., 1999. The Global Land One-Kilometer Base Elevation (GLOBE) Digital Elevation Model. National Oceanic and Atmospheric Administration, National Geophysical Data Center, 325 Broadway, Boulder, Colorado 80305-3328, U.S.A, Version 1.0. URL: http://www.ngdc.noaa.gov/mgg/topo/globe.html.

Hersbach, H., Bell, B., Berrisford, P., Hirahara, S., Horányi, A., Muñoz Sabater, J., Nicolas, J., Peubey, C., Radu, R., Schepers, D., Simmons, A., Soci, C., Abdalla, S., Abellan, X., Balsamo, G., Bechtold, P., Biavati, G., Bidlot, J., Bonavita, M., De Chiara, G., Dahlgren, P., Dee, D., Diamantakis, M., Dragani, R., Flemming, J., Forbes, R., Fuentes, M., Geer, A., Haimberger, L., Healy, S., Hogan, R.J., Hólm, E., Janisková, M., Keeley, S., Laloyaux, P., Lopez, P., Lupu, C., Radnoti, G., de Rosnay, P., Rozum, I., Vamborg, F., Villaume, S., Thépaut, J.N., 2020. The ERA5 global reanalysis. Q. J. R. Meteorol. Soc. 146, 1999–2049. http://dx.doi.org/10.1002/qj.3803.

Hine, D., 1998. Malpensa 2000. Ital. Politics 14, 209–226.

Hong, H., Ye, W., 2014. Estimating extreme wind speed based on regional frequency analysis. Struct. Saf. 47, 67–77. http://dx.doi.org/10.1016/j.strusafe.2013.12.001.

Huang, M., Li, Q., Xu, H., Lou, W., Lin, N., 2018. Non-stationary statistical modeling of extreme wind speed series with exposure correction. Wind Struct. 26, 129–146. http://dx.doi.org/10.12989/was.2018.26.3.129.

Isyumov, N., 2012. Alan G. Davenport's mark on wind engineering. J. Wind Eng. Ind. Aerodyn. 104–106, 12–24. http://dx.doi.org/10.1016/j.jweia.2012.02.007.

Italiavola, 2018. Il vento fa una strage di voli a milano malpensa. URL: https://italiavola.com/2018/03/31/il-vento-fa-una-strage-di-voli-a-milano-malpensa/. (in Italian).

Jacob, D., Teichmann, C., Sobolowski, S., Katragkou, E., Anders, I., Belda, M., Benestad, R., Boberg, F., Buonomo, E., Cardoso, R.M., Casanueva, A., Christensen, O.B., Christensen, J.H., Coppola, E., De Cruz, L., Davin, E.L., Dobler, A., Domínguez, M., Fealy, R., Fernandez, J., Gaertner, M.A., García-Díez, M., Giorgi, F., Gobiet, A., Goergen, K., Gómez-Navarro, J.J., Alemán, J.J.G., Gutiérrez, C., Gutiérrez, J.M., Güttler, I., Haensler, A., Halenka, T., Jerez, S., Jiménez-Guerrero, P., Jones, R.G., Keuler, K., Kjellström, E., Knist, S., Kotlarski, S., Maraun, D., van Meijgaard, E., Mercogliano, P., Montávez, J.P., Navarra, A., Nikulin, G., de Noblet-Ducoudré, N., Panitz, H.J., Pfeifer, S., Piazza, M., Pichelli, E., Pietikäinen, J.P., Prein, A.F., Preuschmann, S., Rechid, D., Rockel, B., Romera, R., Sánchez, E., Sieck, K., Soares, P.M.M., Somot, S., Srnec, L., Sørland, S.L., Termonia, P., Truhetz, H., Vautard, R., Warrach-Sagi, K., Wulfmeyer, V., 2020. Regional climate downscaling over europe: perspectives from the EURO-CORDEX community. Reg. Environ. Change 20, 51. http://dx.doi.org/10.1007/s10113-020-01606-9.

Kasperski, M., 2002. A new wind zone map of Germany. J. Wind Eng. Ind. Aerodyn. 90, 1271–1287. http://dx.doi.org/10.1016/S0167-6105(02)00257-X.

Lettau, H., 1969. Note on aerodynamic roughness-parameter estimation on the basis of roughness-element description. J. Appl. Meteorol. (1962-1982) 8, 828–832. http://dx.doi.org/10.1175/1520-0450(1969)008<0828:NOARPE>2.0.CO;2.

Li, S., Sifton, V., Lundgren, J., McClellan, C., Gibbons, M., 2021. Extreme wind climate of the Arabian Peninsula characterized by using WRF simulation. Weather Clim. Extremes 33, 100330. http://dx.doi.org/10.1016/j.wace.2021.100330.

Lipson, M., Grimmond, S., Best, M., Chow, W.T.L., Christen, A., Chrysoulakis, N., Coutts, A., Crawford, B., Earl, S., Evans, J., Fortuniak, K., Heusinkveld, B.G., Hong, J.W., Hong, J., Järvi, L., Jo, S., Kim, Y.H., Kotthaus, S., Lee, K., Masson, V., McFadden, J.P., Michels, O., Pawlak, W., Roth, M., Sugawara, H., Tapper, N., Velasco, E., Ward, H.C., 2022. Harmonized gap-filled datasets from 20 urban flux tower sites. Earth Syst. Sci. Data 14, 5157–5178. http://dx.doi.org/10.5194/essd-14-5157-2022.

Liu, Y., Zhou, L., Qin, Y., Azorin-Molina, C., Shen, C., Xu, R., Zeng, Z., 2024. Impacts of anemometer changes, site relocations and processing methods on wind speed trends in china. Atmos. Meas. Tech. 17, 1123–1131. http://dx.doi.org/10.5194/amt-17-1123-2024.

Logue, J., 1989. The Estimation of Extreme Wind Speeds over Standard Terrain in Ireland. Technical Report, Technical Note 51, Irish Meteorological Service, Dublin.

Lombardo, F.T., 2021. History of the peak three-second gust. J. Wind Eng. Ind. Aerodyn. 208, 104447. http://dx.doi.org/10.1016/j.jweia.2020.104447.

Lott, J., 2004. The quality control of the integrated surface hourly database. In: Proceedings of the 84th AMS Annual Meeting. Seattle, WA, pp. 5039–5045.

Lucas-Picher, P., Argueso, D., Brisson, E., Tramblay, Y., Berg, P., Lemonsu, A., Kotlarski, S., Caillaud, C., 2021. Convection-permitting modeling with regional climate models: Latest developments and next steps. WIREs Clim. Change 12, e731. http://dx.doi.org/10.1002/wcc.731.

Mellor, G., Yamada, T., 1974. A hierarchy of turbulence closure models for planetary boundary layers. J. Atmos. Sci. 31, 1791–1806. http://dx.doi.org/10.1175/1520-0469(1974)031<1791:AHOTCM>2.0.CO;2.

Miller, C., 2003. A once in 50-year wind speed map for Europe derived from mean sea level pressure measurements. J. Wind Eng. Ind. Aerodyn. 91, 1813–1826. http://dx.doi.org/10.1016/j.jweia.2003.09.024.

Mo, H., Hong, H., Fan, F., 2015. Estimating the extreme wind speed for regions in China using surface wind observations and reanalysis data. J. Wind Eng. Ind. Aerodyn. 143, 19–33. http://dx.doi.org/10.1016/j.jweia.2015.04.005.

Molina, M.O., Gutiérrez, C., Sánchez, E., 2021. Comparison of ERA5 surface wind speed climatologies over Europe with observations from the HadISD dataset. Int. J. Climatol. 41, 4864–4878. http://dx.doi.org/10.1002/joc.7103.

Muñoz Sabater, J., Dutra, E., Agustí-Panareda, A., Albergel, C., Arduini, G., Balsamo, G., Boussetta, S., Choulga, M., Harrigan, S., Hersbach, H., Martens, B., Miralles, D.G., Piles, M., Rodríguez-Fernández, N.J., Zsoter, E., Buontempo, C., Thépaut, J.N., 2021. ERA5-land: A state-of-the-art global reanalysis dataset for land applications. Earth Syst. Sci. Data 13, 4349–4383. http://dx.doi.org/10.5194/essd-13-4349-2021.

NCEI, 2023. Integrated Surface Dataset (Global). National Centers for Environmental Informations, URL: https://www.ncei.noaa.gov/access/search/data-search/global-hourly. (Accessed October 2023).

Nimbus Web, 2018a. 27-30 Ottobre 2018: Scirocco eccezionale, mareggiate e alluvioni in Italia con la tempesta vaia. URL: http://www.nimbus.it/eventi/2018/181031TempestaVaia.htm. (in Italian).

Nimbus Web, 2018b. 7-9 gennaio 2018: Scirocco caldo, piogge record e valanghe sulle alpi occidentali. URL: http://www.nimbus.it/eventi/2018/180110SciroccoValangheAlpiW.htm. (in Italian).

Nimbus Web, 2018c. Fine febbraio-inizio marzo 2018: gelo intenso e tardivo, neve a roma, napoli e bari. URL: http://www.nimbus.it/eventi/2018/180302GeloItalia.htm. (in Italian).

Orlanski, I., 1975. A rational subdivision of scales for atmospheric processes. Bull. Am. Meteorol. Soc. 56, 527–530.

Outten, S., Sobolowski, S., 2021. Extreme wind projections over Europe from the Euro-CORDEX regional climate models. Weather Clim. Extremes 33, 100363. http://dx.doi.org/10.1016/j.wace.2021.100363.

Peng, Z., Tang, R., Jiang, Y., Liu, M., Li, Z.L., 2022. Global estimates of 500 m daily aerodynamic roughness length from MODIS data. ISPRS J. Photogramm. Remote Sens. 183, 336–351. http://dx.doi.org/10.1016/j.isprsjprs.2021.11.015.

Piccolroaz, S., Amadori, M., Toffolon, M., Dijkstra, H.A., 2019. Importance of planetary rotation for ventilation processes in deep elongated lakes: Evidence from Lake Garda (Italy). Sci. Rep. 9. http://dx.doi.org/10.1038/s41598-019-44730-1.

Picozzi, V., Akbaba, A., Avossa, A., Ricciardelli, F., 2022. Correction of historical records to improve the reliability of design wind speeds. Eng. Struct. 265. http://dx.doi.org/10.1016/j.engstruct.2022.114473.

Picozzi, V., Landi, F., Avossa, A., Croce, P., Formichi, P., Ricciardelli, F., 2024. The climatic action uncertainty chain. Eng. Struct. 301, 117357. http://dx.doi.org/10.1016/j.engstruct.2023.117357.

Prein, A., Langhans, W., Fosser, G., Ferrone, A., Ban, N., Goergen, K., Keller, M., Tölle, M., Gutjahr, O., Faser, F., Brisson, E., Kollet, S., Schmidli, J., van Lipzig, N.P.M., Leung, R., 2015. A review on regional convection-permitting climate modeling: Demonstrations, prospects, and challenges. Rev. Geophys. 53, 323–361. http://dx.doi.org/10.1002/2014RG000475.

Raffa, M., Adinolfi, M., Reder, A., Marras, G.F., Mancini, M., Scipione, G., Santini, M., Mercogliano, P., 2023. Very high resolution projections over Italy under different CMIP5 IPCC scenarios. Sci. Data 10, 238. http://dx.doi.org/10.1038/s41597-023-02144-9.

Raffa, M., Reder, A., Marras, G.F., Mancini, M., Scipione, G., Santini, M., Mercogliano, P., 2021. VHR-REA_IT dataset: Very high resolution dynamical downscaling of ERA5 reanalysis over Italy by COSMO-CLM. Data 6. http://dx.doi.org/10.3390/data6080088.

Rapella, L., Faranda, D., Gaetani, M., Drobinski, P., Ginesta, M., 2023. Climate change on extreme winds already affects off-shore wind power availability in Europe. Environ. Res. Lett. 18, 034040. http://dx.doi.org/10.1088/1748-9326/acbdb2.

Raschendorfer, M., 2001. The New Turbulence Parameterization of LM. Technical Report, vol. 1, COSMO Newsletter, pp. 89–97.

Ratto, C., Festa, R., Romeo, C., Frumento, O., Galluzzi, M., 1994. Mass-consistent models for wind fields over complex terrain: The state of the art. Environ. Softw. 9, 247–268. http://dx.doi.org/10.1016/0266-9838(94)90023-X.

Ricciardelli, F., 2023. prEN 1991-1-4:2021: the draft second generation eurocode on wind actions on structures - A personal view. Wind Struct. 37, 79–94. http://dx.doi.org/10.12989/was.2023.37.2.079.

Ritter, B., Geleyn, J., 1992. A comprehensive radiation scheme for numerical weather prediction models with potential applications in climate simulations. Mon. Weather Rev. 120, 303–325. http://dx.doi.org/10.1175/1520-0493(1992)120<0303:ACRSFN>2.0.CO;2.

Rojas-Labanda, C., González-Rouco, F., García-Bustamante, E., Navarro, J., Lucio-Eceiza, E.E., Van der Schrier, G., Kaspar, F., 2023. Surface wind over europe: Data and variability. Int. J. Climatol. 43, 134–156. http://dx.doi.org/10.1002/joc.7739.

Romano, B., Fiorini, L., Marucci, A., Zullo, F., 2020. The urbanization run-up in Italy: From a qualitative goal in the boom decades to the present and future unsustainability. Land 9. http://dx.doi.org/10.3390/land9090301.

Sacré, C., 1993. Estimation des Vitesses Extrêmes du Vent en France Métropolitaine. Technical Report, EN CLI 93.9 R, (in French).

Sacré, C., 2000. Une Nouvelle Estimation des Vitesses Extrêmes du Vent en France Métropolitaine. Technical Report. Rapport CSTB, EN-AEC 00.111 C, (in French).

Sacré, C., 2002. Extreme wind speed in France: the '99 storms and their consequences. J. Wind Eng. Ind. Aerodyn. 90, 1163–1171. http://dx.doi.org/10.1016/S0167-6105(02)00229-5.

Safaei Pirooz, A.A., Flay, R.G., Turner, R., 2021. New Zealand design wind speeds, directional and lee-zone multipliers proposed for AS/NZS 1170.2:2021. J. Wind Eng. Ind. Aerodyn. 208. http://dx.doi.org/10.1016/j.jweia.2020.104412.

Schatzmann, M., Rafailidis, S., Pavageau, M., 1997. Some remarks on the validation of small-scale dispersion models with field and laboratory data. J. Wind Eng. Ind. Aerodyn. 67–68, 885–893. http://dx.doi.org/10.1016/S0167-6105(97)00126-8.

Shen, C., Shen, A., Cui, Y., Chen, X., Liu, Y., Fan, Q., Chan, P., Tian, C., Wang, C., Lan, J., Gao, M., Li, X., Wu, J., 2022. Spatializing the roughness length of heterogeneous urban underlying surfaces to improve the WRF simulation-part 1: A review of morphological methods and model evaluation. Atmos. Environ. 270, 118874. http://dx.doi.org/10.1016/j.atmosenv.2021.118874.

Solari, G., Pagnini, L., 2009. Preliminary elements for an innovative wind map of Italy. In: Proceedings of the 5th European & African Conference on Wind Engineering: Florence Italy, July 19th-23rd 2009.

Spassiani, A.C., Mason, M.S., 2021. Application of self-organizing maps to classify the meteorological origin of wind gusts in Australia. J. Wind Eng. Ind. Aerodyn. 210. http://dx.doi.org/10.1016/j.jweia.2021.104529.

Tarquini, S., Isola, I., Favalli, M., Mazzarini, F., Bisson, M., Pareschi, M.T., Boschi, E., 2007. TINITALY/01: a new triangular irregular network of Italy. Ann. Geophys. 50. http://dx.doi.org/10.4401/ag-4424.

Thépaut, J.N., Dee, D., Engelen, R., Pinty, B., 2018. The copernicus programme and its climate change service. In: IGARSS 2018-2018 IEEE International Geoscience and Remote Sensing Symposium. pp. 1591–1593. http://dx.doi.org/10.1109/IGARSS.2018.8518067.

Tiedtke, M., 1989. A comprehensive mass flux scheme for cumulus parameterization in large-scale models. Mon. Weather Rev. 117, 1779–1800. http://dx.doi.org/10.1175/1520-0493(1989)117<1779:ACMFSF>2.0.CO;2.

Torrielli, A., Repetto, M.P., Solari, G., 2013. Extreme wind speeds from long-term synthetic records. J. Wind Eng. Ind. Aerodyn. 115, 22–38. http://dx.doi.org/10.1016/j.jweia.2012.12.008.

Wieringa, J., 1986. Roughness-dependent geographical interpolation of surface wind speed averages. Q. J. R. Meteorol. Soc. 112, 867–889. http://dx.doi.org/10.1002/qj.49711247316.

Wieringa, J., 1996. Does representative wind information exist? J. Wind Eng. Ind. Aerodyn. 65, 1–12. http://dx.doi.org/10.1016/S0167-6105(97)00017-2.

WMO-No. 1555/2010, 2010. Guidelines for Converting Between Various Wind Averaging Periods in Tropical Cyclone Conditions. Standard, World Meteorological Organization (WMO), Geneva, Switzerland.

WMO-No. 8/2021, 2021. Guide To Meteorological Instruments and Methods of Observation, Standard, eighth ed. World Meteorological Organization (WMO), Geneva, Switzerland.

Wouters, H., Demuzere, M., Blahak, U., Fortuniak, K., Maiheu, B., Camps, J., Tielemans, D., van Lipzig, N., 2016. The efficient urban canopy dependency parametrization (SURY) v1.0 for atmospheric modelling: description and application with the COSMO-CLM model for a Belgian summer. Geosci. Model Dev. 9, 3027–3054. http://dx.doi.org/10.5194/gmd-9-3027-2016.

Xue, Y., Janjic, Z., Dudhia, J., Vasic, R., De Sales, F., 2014. A review on regional dynamical downscaling in intraseasonal to seasonal simulation/prediction and major factors that affect downscaling ability. Atmos. Res. 147–148, 68–85. http://dx.doi.org/10.1016/j.atmosres.2014.05.001.

Yang, S., Chouinard, L.E., Langlois, S., 2022. Hourly wind data for aeolian vibration analysis of overhead transmission line conductors. J. Wind Eng. Ind. Aerodyn. 230. http://dx.doi.org/10.1016/j.jweia.2022.105184.

Yu, J., Stathopoulos, T., Li, M., 2023. Exposure factors and their specifications in current wind codes and standards. J. Build. Eng. 76, 107207. http://dx.doi.org/10.1016/j.jobe.2023.107207.